

MEMS, Field-Emitter, Thermal, and Fluidic Devices

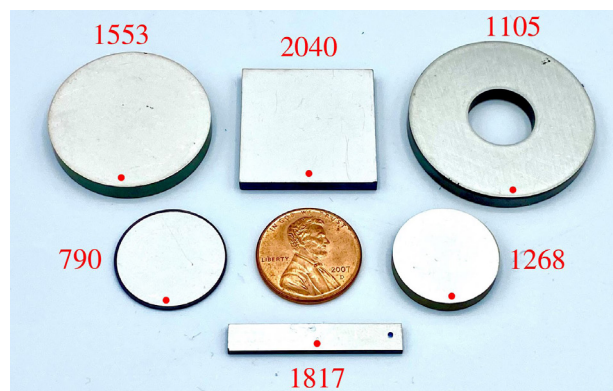
Comparing Piezoelectric Materials and Vibration Modes for Power Conversion	76
Acoustically Active Surface for Automobile Interiors Based on Piezoelectric Dome Arrays.....	77
Advanced Microfluidic Heat Exchangers via 3D Printing and Genetic Algorithms	78
3D-Printed Miniature Vacuum Pumps	79
3D-Printed, Miniaturized Retarding Potential Analyzers for Cubesat Ionospheric Studies	80
Multi-Dimensional Double Spiral Device for Fully Automated Sample Preparation.....	81
Internally Fed, Additively Manufactured Electro spray Thruster.....	82
Planar Field-Emission Electron Sources via Direct Ink Writing	83
Micro Rocket Engine Using Steam Injector and Electric Fuel Pump	84
Nonvolatile Electrically Reconfigurable Photonic Circuits Based on Low-Loss Phase-Change Materials	85
Extremely Dense Arrays of Si Emitters with Self-Aligned Extractor and Focusing Gates.....	86
Gated Silicon Field-Ionization Arrays for Compact Neutron Sources.....	87
Field Emission from a Single Nanotip in Controlled Poor Vacuum.....	88
GaN Vertical Nanostructures Sharpened by A New Digital Etching Process for Field Emission Applications	89
Integrating Object Form and Electronic Function in Rapid Prototyping and Personal Fabrication	90
MEMS Energy Harvesting and AI-based Design Processing.....	91

Comparing Piezoelectric Materials and Vibration Modes for Power Conversion

J. D. Boles, J. E. Bonavia, P. L. Acosta, Y. K. Ramadass, J. H. Lang, D. J. Perreault
Sponsorship: Texas Instruments, NSF GRFP, Enphase Energy, Masdar Institute

Major industries such as transportation, energy systems, manufacturing, healthcare, consumer electronics, and information technology vitally depend on power electronics for processing electrical energy. Power electronics are often the bulkiest components in the systems they serve, and smaller converter designs are typically limited by magnetic energy storage components (i.e., inductors and transformers). The power density and efficiency capabilities of magnetics fundamentally decrease at low volumes, which motivates exploration of other energy storage mechanisms that are more conducive to miniaturization.

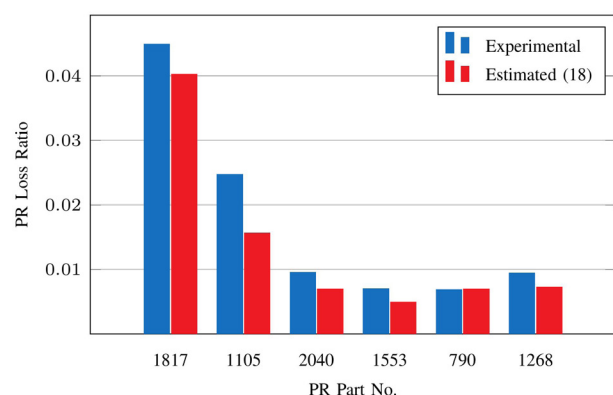
One promising alternative is piezoelectric energy storage; piezoelectrics store energy in the mechanical compliance and inertia of a piezoelectric material, and they offer several potential advantages to power conversion. In previous work, we have demonstrated a converter implementation capable of >99% peak efficiency using a commercially available piezoelectric resonator (PR). However, criteria for selecting piezoelectric materials and/or designing PRs themselves remain murky in the context of power conversion.



▲ Figure 1: PRs tested for experimental validation of efficiency FOMs, with APC International part numbers shown in red. These PRs represent four different PZT materials and span four vibration modes.

In this work, we derive figures of merit (FOMs) for piezoelectric materials and vibration modes specifically for use in power electronics. In particular, we focus on maximum efficiency and maximum power density FOMs for PRs in realistic converter switching sequences. These FOMs are shown to depend on only material properties for each of seven vibration modes, and they correspond to specific PR geometry conditions for realizing both maximum efficiency and maximum power density in PR designs.

We validate these FOMs and their geometry conditions using a numerical solver for converter operation as well as experimental results for six commercially available PRs (shown in Figures 1-2). The proposed FOMs are demonstrated to be highly representative metrics for PR efficiency and power density capabilities, and these properties are likewise shown to scale favorably for converter miniaturization. Thus, by enabling smaller-volume converters, piezoelectrics are positioned to both reduce system costs and open new application spaces for power conversion.



▲ Figure 2: Experimental minimum loss ratio of the PRs in Figure 1 compared to the estimate provided by the efficiency FOMs.

FURTHER READING

- J. D. Boles, J. J. Piel, and D. J. Perreault, "Enumeration and Analysis of DC-DC Converter Implementations Based on Piezoelectric Resonators," *IEEE Transactions on Power Electronics*, vol. 36, no. 1, pp. 129-145, 2021.
- J. D. Boles, J. E. Bonavia, P. Acosta, Y. K. Ramadass, J. H. Lang, and D. J. Perreault, "Evaluating Piezoelectric Materials and Vibration Modes for Power Conversion" (submitted).
- J. D. Boles, P. Acosta, Y. K. Ramadass, J. H. Lang, and D. J. Perreault, "Evaluating Piezoelectric Materials for Power Conversion," *IEEE Workshop on Control and Modeling for Power Electronics (COMPEL)*, Aalborg, Denmark, Nov. 2020.

Acoustically Active Surface for Automobile Interiors Based on Piezoelectric Dome Arrays

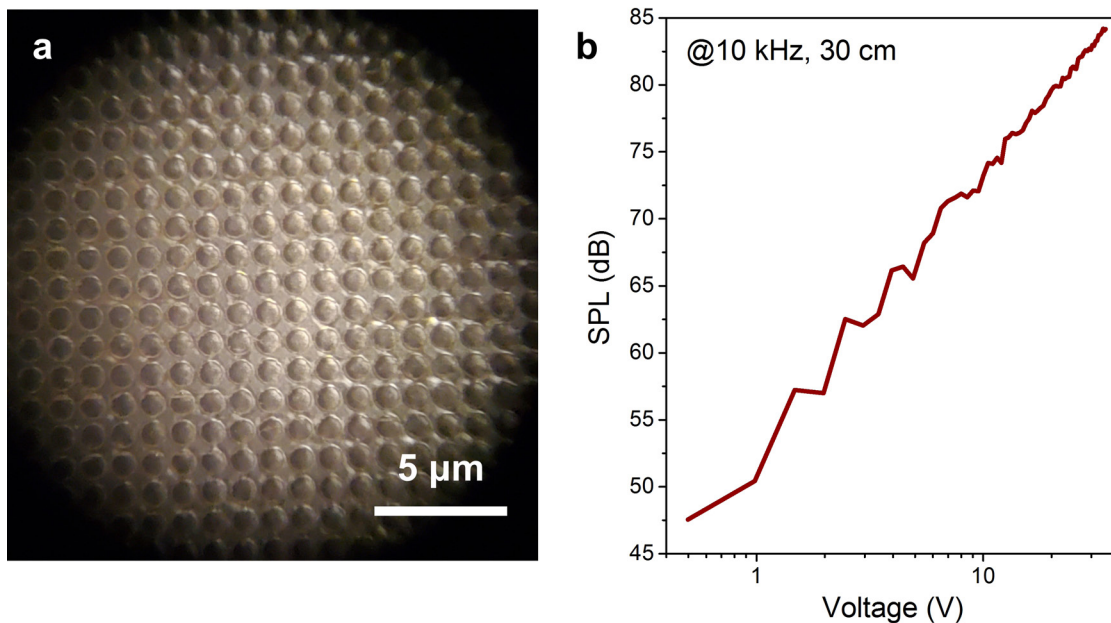
J. Han, J. Lang, V. Bulović

Sponsor: Ford Motor Company

The surfaces of automobile interiors can be rendered acoustically active by mounting on them flexible, wide-area thin-films with arrays of small acoustic transducers. Each small, individually addressable transducer functions as a speaker, a microphone, or an ultrasonic transceiver. Engineering the structures and dimensions of individual transducers on the acoustic surface offers widely tunable performance. Coordinating the phased transducer array based on adaptive control could enable unique functionalities of the acoustic surface such as directional sound generation and detection. As a result, the acoustically active surface can work either in the audio frequency range for noise cancellation, personal entertainment, and communication with the vehicle or in the ultrasound frequency range for gesture detection, alertness monitoring, etc., which collectively improve the comfort and safety of the automobile.

This project seeks to develop and demonstrate a wide-area, paper-thin, robust, and even transparent

acoustic surface based on an array of dome-shaped piezoelectric transducers. Dependencies of the acoustic performance on the design variables of the piezoelectric domes are studied through theoretical modeling, simulation, and experimental characterization of dome vibration and sound radiation by the acoustic surface. A 12- μm -thick, $10\times 10\text{ cm}^2$ acoustic surface consisting of an array of polyvinylidene difluoride (PVDF) can be further enhanced by scaling up the area, utilizing superior piezoelectric materials, enlarging the dome size, and/or reducing the film thickness. A scalable micro-embossing process has been developed to fabricate the small domes with high precision and at low cost. $10\times 10\text{ cm}^2$ samples (Figure 1) were prepared with different dome dimensions and tested in an anechoic chamber. The results confirm outstanding performance of the acoustic surface, owing to the existence of active microstructures in an array, and thereby show great promise for broad application scenarios.



▲ Figure 1: (a) Microscopic image of a $10\times 10\text{ cm}^2$ sample of the acoustic surface based on embossed PVDF domes. (b) Free-field sound generation of the acoustic surface under 10 kHz at 30 cm away.

Advanced Microfluidic Heat Exchangers via 3D Printing and Genetic Algorithms

J. Izquierdo-Reyes, L.F. Velásquez-García

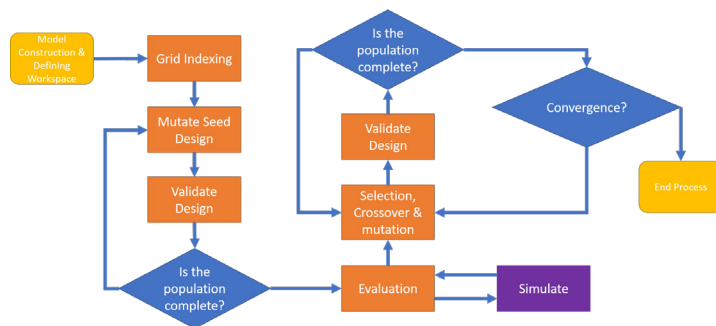
Sponsorship: MIT-Tecnologico de Monterrey Nanotechnology Program

Power electronics are fundamental in many high-tech applications, e.g., electric cars. Adequate heat dissipation of these electronic components is essential for them to operate properly and attain long lifespans. Cooling high-power electronics typically employs heat exchangers that put a liquid in contact with hot surfaces to extract heat. Using microfluidics can greatly increase the surface-to-volume ratio of the liquid, boosting heat transfer. However, classically designed heat exchangers do not properly address the non-uniformity of the heat field, e.g., localized hot spots. In addition, better power microelectromechanical system microfluidics can be created via additive manufacturing, involving better materials and implementing more effective geometries than in mainstream cleanroom microfabrication. In particular, metal 3D printing can monolithically create complex microfluidic devices while greatly simplifying the manufacturing process and requiring significantly less time than subtractive manufacturing.

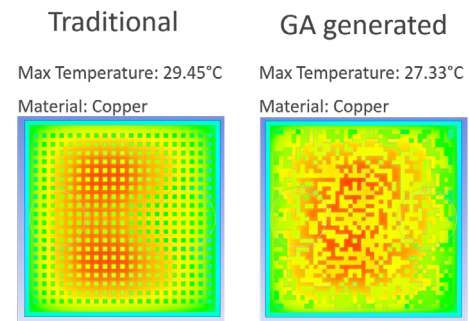
Genetic algorithms (GAs) can be used to implement an iterative design process inspired in natural selection that can potentially create better engineering solutions by generating unexpected

implementations. In a nutshell, GAs are used to create multiple generations of randomized mutations of the parent designs (called subjects), looking to optimize the solution's performance by minimizing/maximizing a particular fitness function.

In this project, we are exploring metal 3D printing and GAs to implement better microfluidic heat exchangers. The fitness function employed ponders trade-offs between temperature and pressure drop in the cold plate to minimize the maximum temperature. We use a finite element solver with a computational fluid dynamics module to obtain solutions of the flow and temperature fields of each subject of each generation and then we used software to compare their performance across each generation and down-select the best designs. The software creates and analyzes new generations until it attains a certain threshold value in the fitness function (Figure 1). The resultant devices are complex, often counter-intuitive, and unlikely to be synthesized by a human using first principles (Figure 2), surpassing the performance of traditional designs.



▲ Figure 1: Block diagram of the algorithm employed to design advanced microfluidic heat exchangers.



▲ Figure 2: Classically designed (left) and GA-designed (right) finned cold plate for a CPU chip. A reduction of 2.12 °C in the maximum device temperature was attained.

FURTHER READING

- E. Segura-Cárdenas and L. F. Velásquez-García, "Additively Manufactured Robust Microfluidics via Silver Clay Extrusion," *J. Microelectromech. Syst.*, vol. 29, no. 3, pp. 427-437, Jun. 2020.
- Z. Sun and L. F. Velásquez-García, "Monolithic FFF Printed, Biodegradable, Biocompatible, Dielectric-Conductive Microsystems," *J. Microelectromech. Syst.*, vol. 26, no. 6, pp. 1356-1370, Dec. 2017.
- A. L. Beckwith, J. T. Borenstein, and L. F. Velásquez-García, "Monolithic, 3D-printed Microfluidic Platform for Recapitulation of Dynamic Tumor Microenvironments," *J. Microelectromech. Syst.*, vol. 27, pp. 1009-1022, Oct. 2018.

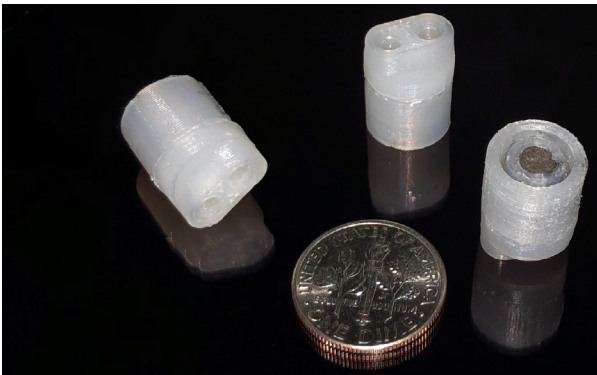
3D-Printed Miniature Vacuum Pumps

A. P. Taylor, J. Izquierdo-Reyes, L.F. Velásquez-García
Sponsorship: Edwards Vacuum, MIT-Tecnologico de Monterrey Nanotechnology Program

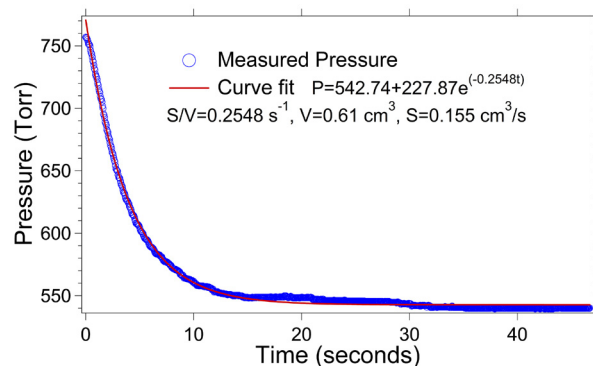
Compact pumps that create and sustain vacuum environments while supplying precise gas flow rates are essential to implement a variety of microsystems. Positive displacement vacuum pumps, e.g., diaphragm pumps, create and maintain vacuum by cycling pockets of gas that are compressed from rarified conditions to atmospheric pressure. Miniaturized positive displacement vacuum pumps typically have dead volumes very similar to the maximum displacement of their compression chambers, resulting in the creation of modest vacuums.

Magnetic, long-stroke actuators could be used to implement pump chambers with large compression ratios; an exciting possibility to implement such actuators at a low cost is additive manufacturing. In this project, we demonstrated the first miniaturized, additively manufactured, magnetic diaphragm pumps for liquids in the literature where all constitutive parts, including the magnets, are monolithically 3D-printed. The devices were created in nylon-based feedstock via fused filament fabrication, in which thermoplastic

filament was extruded from a hot nozzle to create a solid object layer by layer. The miniature pumps use 150- μm - or 225- μm - thick membranes connected to a piston with an embedded magnet, a chamber, two diffusers, and two fluidic connectors (Figure 1). We also experimentally observed that the same pumps for liquids can be used as vacuum pumps if they are first moistened with a small amount of water to enable the pump diffusers to seal during actuation. The miniature 3D-printed pumps can attain an ultimate pressure of 540 Torr at an operating frequency of 230 Hz, i.e., the pumps achieve a pressure of 220 Torr below atmospheric pressure (Figure 2). The ultimate pressure achieved by our pumps is close to values reported from commercially available, non-microfabricated, miniature diaphragm pumps with comparable diaphragm diameters. We speculate that changing the design of the pump chamber to increase its compression ratio and printing a more flexible and compliant material could attain lower ultimate pressure.



▲ Figure 1: 3D-printed miniature magnetic pumps next to a US dime; the fluidic ports and the embedded magnet are visible at either end of the pumps.



▲ Figure 2: Pressure versus time characteristic of a 3D-printed magnetic pump (from A. P. Taylor, J et al., *J. Phys. D: Appl. Phys.*, vol. 53, no. 35-5002, Jun. 2020). Data in blue, exponential curve fit in red.

FURTHER READING

- A. P. Taylor, C. Velez Cuervo, D. P. Arnold, and L. F. Velásquez-García, "Fully 3D-printed, Monolithic, Mini Magnetic Actuators for Low-cost, Compact Systems," *J. Microelectromech. Syst.* vol. 28, no. 3, pp. 481-493, Jun. 2019.
- A. P. Taylor and L. F. Velásquez-García, "Miniaturized Diaphragm Vacuum Pump by Multi-Material Additive Manufacturing," *J. Microelectromech. Syst.*, vol. 26, no. 6, pp. 1316 - 1326, Dec. 2017.
- A. P. Taylor, J. Izquierdo-Reyes, and L. F. Velásquez-García, "Compact, Magnetically Actuated, Additively Manufactured Pumps for Liquids and Gases," *J. Phys. D: Appl. Phys.*, vol. 53, no. 35-5002, Jun. 2020.

3D-Printed, Miniaturized Retarding Potential Analyzers for Cubesat Ionospheric Studies

J. Izquierdo-Reyes, L.F. Velásquez-García

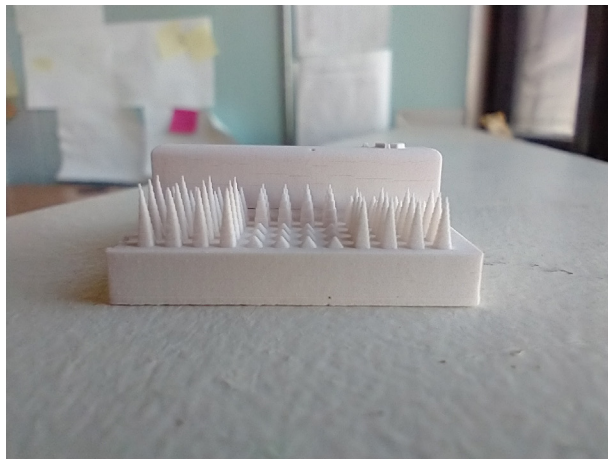
Sponsorship: MIT-Portugal, MIT-Tecnologico de Monterrey Nanotechnology Program

The ionosphere is an upper region of the atmosphere that is made of plasma created and sustained by solar UV radiation. Little is known about some of the layers of the ionosphere, e.g., the thermosphere. Comprehending the processes taking place in the thermosphere is essential to understand local and global weather and global warming. There is evidence that global warming is cooling down the thermosphere, causing serious issues, e.g., variation in satellites' drag and less recycling of water. In-situ data would provide more and better information.

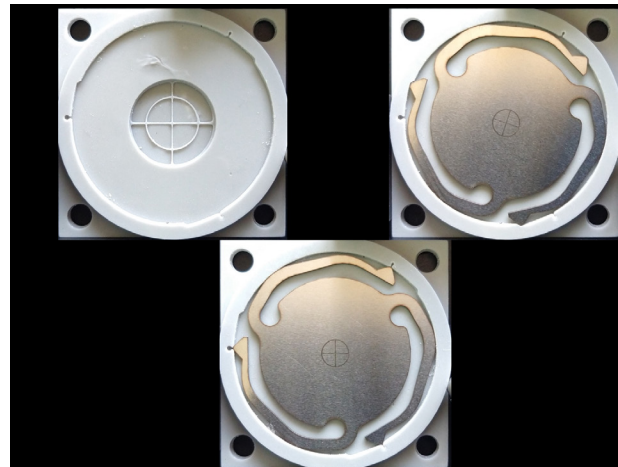
Plasma sensors are used to characterize plasmas, measuring one or more properties that can be derived from the position and velocity distributions of the particles that make up the plasma. A retarding potential analyzer (RPA) is a multi-gridded sensor that measures the ion energy distribution of a plasma. In an RPA, the diameter of the apertures of the outermost grid (the floating grid) measures up to two Debye lengths to trap the plasma outside the sensor while the inter-grid spacing measure up to four Debye lengths to avoid space charge effects that would smear the measurements. The Debye length in the ionosphere is about 1 mm.

Sending hardware to space is quite expensive because, among other reasons, of the physics of rocket propulsion, e.g., requiring ejecting propellant many times the mass of the spacecraft. Therefore, technologies that yield smaller, lighter, and cheaper space hardware without sacrificing performance are of great interest. Consequently, there is great interest in developing mission-focused miniaturized satellites, i.e., cubesats (1-10 Kg, a few L in volume).

In this project we are harnessing additive manufacturing to demonstrate better and cheaper cubesat plasma sensors. Our RPA design uses laser-micromachined stainless steel grids integrated to a 3D-printed ceramic housing made via vat polymerization using 60- μm by 60- μm by 100- μm XYZ voxels (Figure 1). Each grid is assembled to the housing using a set of engineered springs that provide active alignment. Experiments show that the per-level assembly precision is better than 100 μm (Figure 2). Inter-grid alignment results in larger current signals. Current work focuses on completing, fabricating, and characterizing the RPA design.



▲ Figure 1: Example of a 3D-printed ceramic resolution matrix. The width of the piece facing the camera is about 60 mm.



▲ Figure 2: Selected views of an assembly misalignment experiment: a) ceramic grid holder with spring interacting features, b) metallic grid before spring actuation, c) metallic grid with actuated and locked-in springs.

FURTHER READING

- E. Heubel and L. F. Velásquez-García, "Microfabricated Retarding Potential Analyzers with Enforced Aperture Alignment for Improved Ion Energy Measurements in Plasmas," *J. Microelectromech. Syst.* vol. 24, no. 5, pp. 1355-1369, 2015.
- Z. Sun, G. Vladimirov, E. Nikolaev, and L. F. Velásquez-García, "Exploration of Metal 3-D Printing Technologies for the Microfabrication of Freeform, Finely Featured, Mesoscaled Structures," *J. Microelectromech. Syst.*, vol. 27, no. 6, pp. 1171 – 1185, Dec. 2018
- C. Yang and L. F. Velásquez-García, "Low-Cost, Additively Manufactured Electron Impact Gas Ionizer with CNT Field Emission Cathode for Compact Mass Spectrometry," *J. Phys. D – Appl. Phys.* vol. 52, no. 7, 075301 (9pp), Feb. 2019.

Multi-Dimensional Double Spiral Device for Fully Automated Sample Preparation

H. Jeon, J. Han

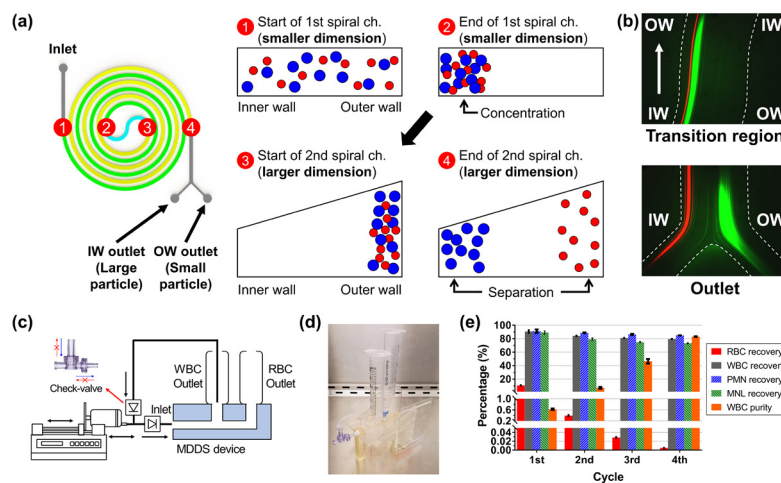
Sponsorship: NIH, Ohana Bioscience

Sample preparation is the process of extracting target analytes from interferents for the sensitive and successful downstream analysis of samples. To overcome the limitations of the current standard (centrifugation), which entails many energy-consuming steps, various microfluidic devices have been developed. Among them, the inertial spiral microfluidic device has been extensively utilized due to its inherent advantages including label-free, high-throughput, and reliable operation without any external force field. However, improvement of separation efficiency and usability is required for field-deployable applications.

In response to this critical need, we developed a new type of spiral device, the multi-dimensional double spiral (MDDS) device. The MDDS device is composed of two sequentially connected spiral channels having different dimensions. Particles can be concentrated through the first, smaller-dimensional spiral channel and subsequently separated through the second, larger-dimensional spiral channel (Figure 1a). The initial focusing in the first spiral channel can significantly de-

crease particle dispersion and effectively extract smaller particles into the outer-wall side of the channel, increasing separation resolution and efficiency (Figure 1b).

To achieve more purified and concentrated output, we also developed a new recirculation platform based on a check-valve which allows only one-way flow. In the platform, an output from the MDDS separation can be extracted back into the input syringe and processed again repeatedly via programmed back-and-forth motions of a syringe pump, resulting in higher purity and concentration (Figure 1c). The developed platform can be operated in a fully automated or even hand-powered manner. Using the platform, we successfully demonstrated the isolation of white blood cells from a diluted blood sample by removing abundant red blood cells (up to 99.99%). We expect that the developed platform could provide an innovative field-deployable sample preparation solution to point-of-care sample analyses (not limited to blood) and diagnostics.



▲ Figure 1: (a) A schematic diagram of the MDDS device and its operation. (b) Trajectories of 6- μm (green) and 10- μm (red) particles. (c) A schematic and (d) an image of the check-valve-based recirculation platform. (e) Recoveries and purity of blood cells from 4 cycles of recirculation.

FURTHER READING

- H. Jeon, B. Jundi, K. Choi, H. Ryu, B. D. Levy, G. Lim, and J. Han, "Fully-automated and Field-deployable Blood Leukocyte Separation Platform Using Multi-dimensional Double Spiral (MDDS) Inertial Microfluidics," *Lab Chip*, vol. 20, pp. 3612–3624, 2020. <https://doi.org/10.1039/DoLCo0675K>

Internally Fed, Additively Manufactured Electro spray Thruster

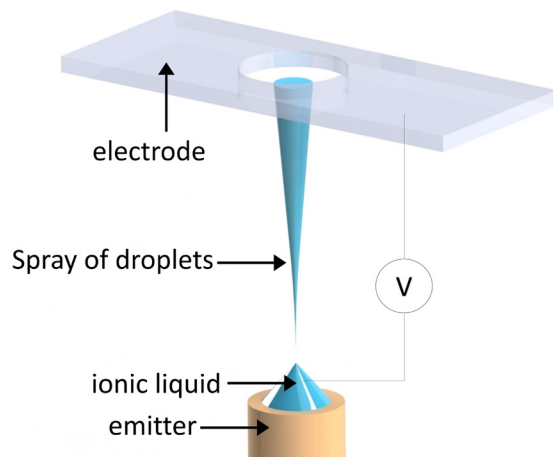
H. Kim, L. F. Velásquez-García
Sponsorship: MIT Portugal

Electrospray engines produce thrust by electrohydrodynamically ejecting high-speed ions or droplets. Electro spray emitters work better if miniaturized because their start-up voltage decreases with the square root of the emitter diameter. A single emitter has very low thrust; multiplexing the emitters, so they uniformly operate in parallel, makes it possible to increase the thrust delivered. Electro spray thrusters are typically created via precision subtractive manufacturing techniques, which is time-consuming and expensive. For New Space, i.e., the development of a commercial space industry, additive manufacturing is an attractive possibility to create complex hardware that is inexpensive and exquisitely iterated and optimized.

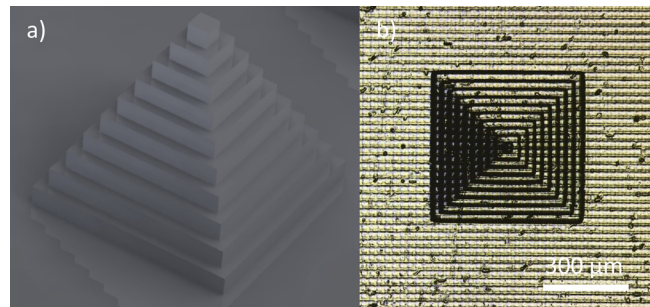
Our group recently demonstrated the first additively manufactured ionic liquid electro spray thrusters in the literature; these devices attain pure ion emission in both polarities, maximizing their specific impulse. However, the propellant flow rate, which has an upper bound for pure ionic emission, limits the thrust per emitter that can be attained for a given bias voltage. An engine that can deliver larger per-emitter

thrust, at the expense of using less efficiently the propellant, is of interest for impulsive maneuvers.

Consequently, we are also interested in developing additively manufactured, low-specific impulse, high per-emitter thrust electro spray engines. Unlike the externally fed, nanoporous fluidic structure used in the ionic thrusters previously described, an internally fed emitter architecture is a better fit to produce droplets (Figure 1), which are heavier than ions, resulting in higher per-emitter thrust. We use the vat polymerization method called digital light processing to make emitters with narrow channels that provide high hydraulic resistance. Using resolution matrices drawn in $\sim 25 \mu\text{m}$ voxels and a resin chemically resistant to an ionic liquid, we verified the high fidelity of the printed parts to the computer-aided design (CAD) models (Figure 2). Current research efforts focus on exploring the resolution limits of the printable feedstock for solid and negative features and developing device designs with hydraulic networks that provide a high and uniform hydraulic impedance to each emitter.



▲ Figure 1: Schematic of a single internally fed electro spray emitter.



▲ Figure 2: a) CAD image and b) confocal microscope image of printed part for one of the test structures used to verify printing fidelity.

FURTHER READING

- F. A. Hill, E. V. Heubel, P. P. de Leon, and L. F. Velásquez-García, "High-Throughput Ionic Liquid Ion Sources Using Arrays of Microfabricated Electro spray Emitters with Integrated Extractor Grid and Carbon Nanotube Flow Control Structures," *J. of Microelectromechanical Systems*, vol. 23, no. 5, pp. 1237-1248, May, 2014.
- D. Olvera-Trejo and L. F. Velásquez-García, "Additively Manufactured MEMS Multiplexed Coaxial Electro spray Sources for High-Throughput, Uniform Generation of Core-Shell Microparticles," *Lab on a Chip*, vol. 16, no. 21, pp. 4121-4132, Oct. 2016.
- D. V. Melo Maximo, and L. F. Velásquez-García, "Additively Manufactured Electrohydrodynamic Ionic Liquid Pure-Ion Sources for Nanosatellite Propulsion," *Additive Manufacturing*, vol. 36, p. 101719, Dec. 2020.

Planar Field-Emission Electron Sources via Direct Ink Writing

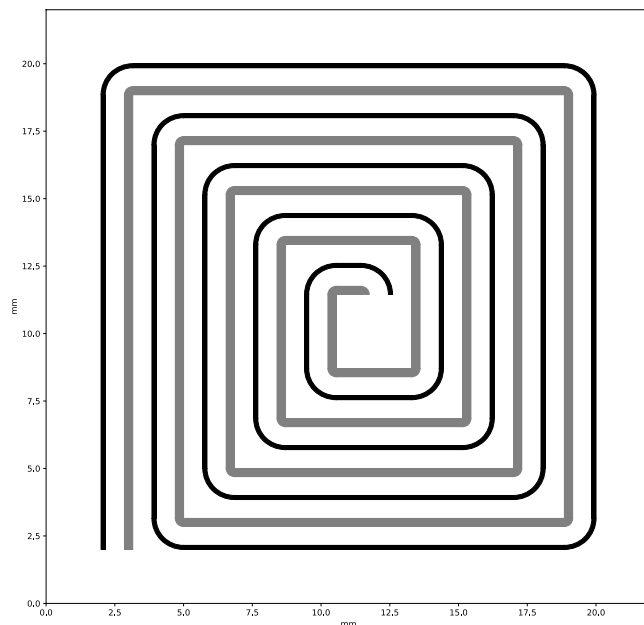
N. Klugman, L. F. Velásquez-García
Sponsorship: MIT Portugal

Vacuum electron sources appear in numerous technologies, from microscopy to displays to mass spectrometry. The two main forms vacuum electron sources can take are thermionic and field emission. Thermionic sources emit electrons by raising the temperature of a conductor so that many of its electrons have an energy greater than the potential barrier trapping them, allowing them to escape. Field-emission sources use an applied electric field to lower the potential barrier, allowing electrons to quantum tunnel out of the conductor. Field-emission sources can therefore operate at lower temperatures, in a poorer vacuum, faster, and using less energy, all of which increase the usability of the electron source.

Field-emission sources' emitting electrodes have been made from many materials, but research has focused on carbon nanotubes (CNTs). CNTs' nanosized tips and high aspect ratio lead to high electric fields at modest voltages, which is useful since the emitted current increases with electric field; in

addition, CNTs have excellent chemical resistance, e.g., resisting oxidation by the trace gases in the vacuum. Manufacturing CNT field-emission sources is often a costly and time-intensive effort, particularly when the CNT growth locations are restricted by desired device geometry.

To affordably implement CNT field emission cathodes, this project explores direct ink writing to create in-plane, gated field-emission sources. A spiral CNT ink trace is printed on an insulating substrate, along with a symmetric, co-planar trace (see Figure 1) of a different conducting (e.g., silver nanoparticle) ink. A voltage applied between the traces induces an electric field, causing electron tunneling from the CNT tips. The planar design reduces manufacturing complexity and increases electron transmission. Current work includes printable feedstock material selection, exploration of geometric modifications to increase device longevity, and increasing imprint density to allow for greater emission current density.



◀ Figure 1: Computer-aided design of 3D-printed field-emission cathode with in-plane gate.

FURTHER READING

- A. Perales and L. F. Velásquez-García, "Fully 3D-Printed Carbon Nanotube Field Emission Electron Sources with In-plane Gate Electrode," *Nanotechnology*, vol. 30, no. 49, p. 495302, Dec. 2019
- C. Yang and L. F. Velásquez-García, "Low-cost, Additively Manufactured Electron Impact Gas Ionizer with CNT Field Emission Cathode for Compact Mass Spectrometry," *Journal of Physics D – Applied Physics*, vol. 52, no. 7, p. 075301, Feb. 2019.
- L. F. Velásquez-García, A. I. Akinwande, and M. Martínez-Sánchez, "Precision Hand Assembly of MEMS Subsystems Using DRIE-patterned Deflection Spring Structures: An Example of an Out-of-Plane Substrate Assembly," *Journal of Microelectromechanical Systems*, vol. 16, no. 3, pp. 598 – 612, Jun. 2007.

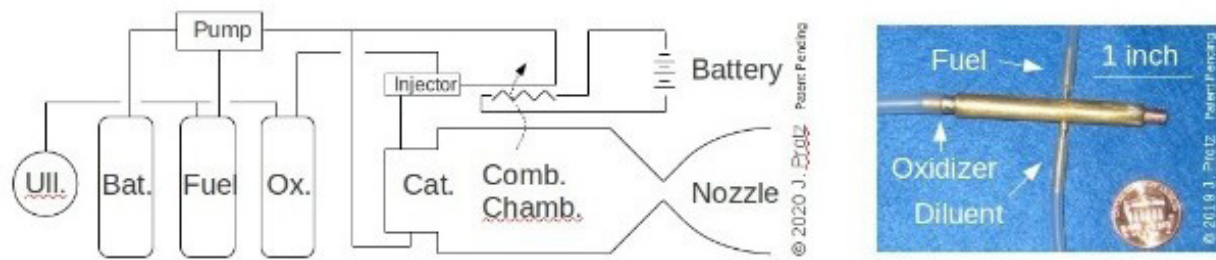
Micro Rocket Engine Using Steam Injector and Electric Fuel Pump

J. Protz

Sponsorship: Protz Lab Group; microEngine, LLC

Micro-fabricated miniature chemical rocket engines have been an active area of research at MIT and elsewhere for two decades; they are a compelling propulsion option for small launch vehicles and spacecraft. At these scales, miniaturized steam injectors like those used in Victorian-era steam locomotives are viable as a pumping mechanism and offer an alternative to pressure feed and high-speed turbo-pumps. Storing propellants at low pressure reduces tank mass, and this improves the vehicle empty-to-gross mass ratio; if one propellant is responsible for most of the propellant mass (e.g., oxidizer), injecting it while leaving the others solid or pressure-fed can still achieve much of the potential gain. Previously, the principal investigator and his group built and tested ultraminiature-machined micro jet injectors that pumped ethanol and explored pressure-fed liquid and hybrid engine designs. Current

work has focused on configurations that use a battery and electric pump to replace the pressure-feed portion of past designs; electric pumps pump fuel and/or coolant while a steam injector motivated by boiled coolant pumps the oxidizer. This replacement allows pressurized tanks to be avoided altogether, greatly simplifying implementation and the sourcing of components while still being compatible with miniaturization via a micro-electromechanical system (MEMS). Current work has focused on designing and implementing an axisymmetric whole-engine mock-up or test article that simultaneously integrates a steam injector, boiler, decomposition chamber, fuel injector, thrust chamber, and electric fuel pump while being practical to build and also retaining compatibility with 2D MEMS fabrication (see Figure 1).



▲ Figure 1: (a) Schematic representation of engine and (b) engineering mock-up in brass of an integrated engine (w/o electric pump).

FURTHER READING

- J. M. Protz, "Steam-Injector and Electric Micro Rocket," presented at *Gas Turbine Laboratory Seminar*, MIT, Cambridge, MA, Nov. 17, 2020.
- J. Protz, "Hybrid and Partially Pressure-Fed Injector-Pumped Micro Rockets," (JANNAF 2019-004BT), presented at the *Joint Army-Navy-NASA-Air Force Joint Meeting of the 13th Modeling and Simulation / 11th Liquid Propulsion / 10th Spacecraft Propulsion Subcommittees and Meeting of the Programmatic and Industrial Base (JANNAF)*, Tampa, FL, Dec. 9-13, 2019.
- J. M. Protz, "Modeling and Analysis of a Giffard-Injector-Pumped Bipropellant Microrocket," invited talk at *Pratt & Whitney Rocketdyne*, Huntsville, AL, Feb. 3, 2010.

Nonvolatile Electrically Reconfigurable Photonic Circuits Based on Low-Loss Phase-Change Materials

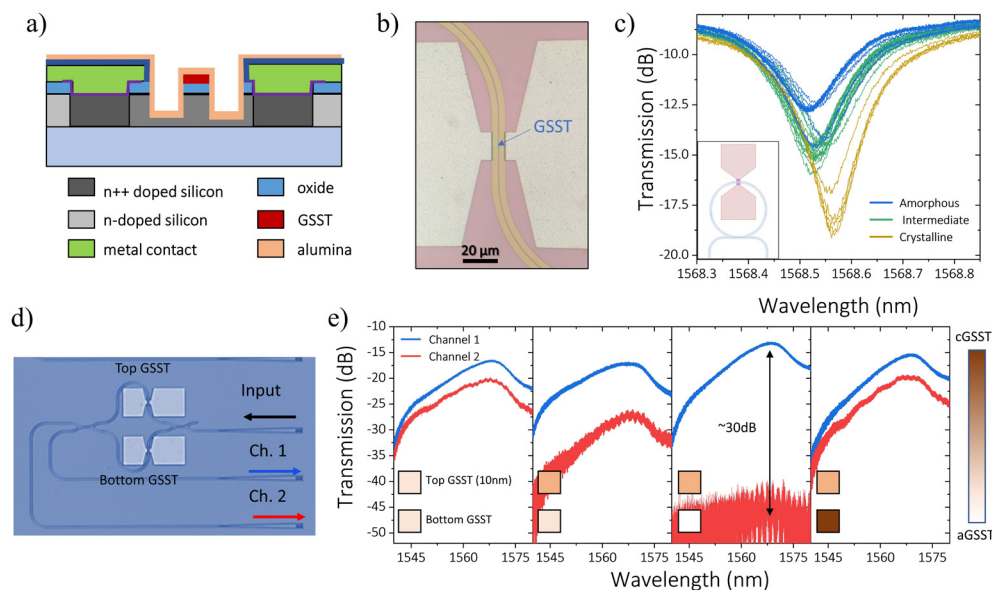
C. Ríos, Q. Du, Y. Zhang, M. Shalaginov, P. Miller, P. Robinson, C. Roberts, T. Gu, S. Vitale, J. Hu
Sponsorship: DARPA

Low-power active components are crucial to achieving programmable photonic integrated circuits (PICs). Reaching this goal drives the development of active components with outstanding performance in the gigahertz-frequency operation required in telecommunication applications but also on slower scales for active reconfiguration of PICs. However, these components are all volatile, which is not ideal for applications where the configurations are performed sporadically or just once. In the latter case, nonvolatile reconfiguration capable of retaining any configuration with zero-power consumption is the desired functionality. To fill this gap, we employ $\text{Ge}_2\text{Sb}_2\text{Se}_4\text{Te}_1$ (GSST), a low-loss broadband optical phase-change material. GSST allows refractive index modulation by using a heat stimulus to switch between the amorphous and the crystalline states, which results in an outstanding modulation of optical properties ($\Delta n \sim 1.7$).

We patterned $\sim 10^{18} \text{ cm}^{-3}$ n-doped silicon microheaters to provide the heat stimuli and electrothermally configure the state of GSST, which was

evanescently coupled to the propagating mode of a half-etched rib waveguide (Figure 1). We evaporated 30 nm of GSST, which theoretically introduced a π phase-shift with a 5- μm -long cell. We demonstrated 50 cycles of reversible and repeatable switching between the amorphous and two partially crystallized states of a 3- μm -long GSST and the subsequent phase shift on a ring resonator (Figure 1c). We used $3.5\text{V} \times 20 \text{ ms}$ and $5\text{V} \times 50 \mu\text{s}$ pulses to crystallize and amorphize, respectively. Our analysis reveals that doped Si contributes only to 0.03 dB/ μm absorption, amorphous GSST shows zero loss, and crystalline GSST shows 0.57 dB/ μm .

Furthermore, we demonstrate GSST-based phase-shifters on a balanced 2×2 MZI switch structure (Figure 1d, Figure 1e). We measured the variations on the two output channels as a function of the state of a 10- μm -long GSST in each arm. Using the same pulse sequence as above, we achieved $\pi/2$ phase-shift upon amorphization followed by full recrystallization with a 30-dB extinction ratio.



▲ Figure 1: a) Sketch of the GSST-based device using n-doped silicon heaters. b) Image of a 10- μm -long microheater with 3- μm -long, 30-nm-thick GSST covering the waveguide. c) Resonance peak for three distinct GSST states on a ring with 120- μm radius; each line represents a switching event. d) Image of a MZI switch with two 80/20-splitting directional couplers and two GSST phase shifters. e) Spectra recorded for both channels under different GSST configurations in a 10- μm -long GSST/20- μm -long microheater.

FURTHER READING

- M. Wuttig, H. Bhaskaran, and T. Taubner, "Phase-change Materials for Non-volatile Photonic Applications," *Nat. Photonics*, vol. 11, pp. 465–476, 2017.
- Y. Zhang, J. B. Chou, J. Li, H. Li, Q. Du, A. Yadav, S. Zhou, M. Y. Shalaginov, Z. Fang, H. Zhong, C. Roberts, P. Robinson, B. Bohlin, C. Rios, H. Lin, M. Kang, T. Gu, J. Warner, V. Liberman, K. Richardson, and J. Hu, "Broadband Transparent Optical Phase Change Materials for High-performance Nonvolatile Photonics," *Nat. Comms.*, vol. 10, p. 4279, 2019.

Extremely Dense Arrays of Si Emitters with Self-Aligned Extractor and Focusing Gates

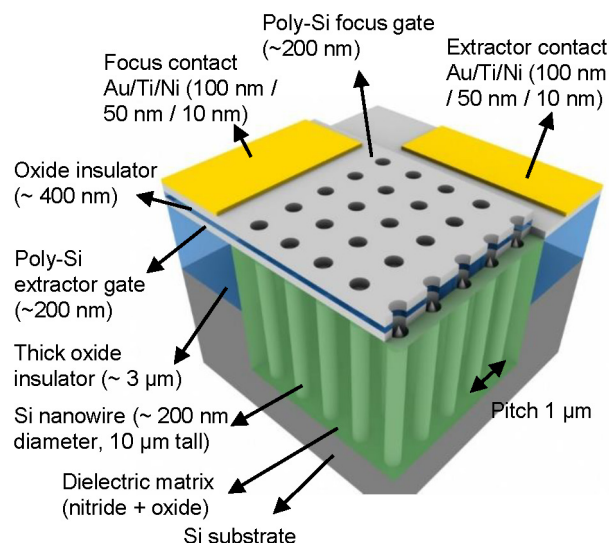
G. Rughoobur, L. Jain, A. I. Akinwande

Sponsorship: Air Force Research Laboratory, Intelligence Advanced Research Projects Activity

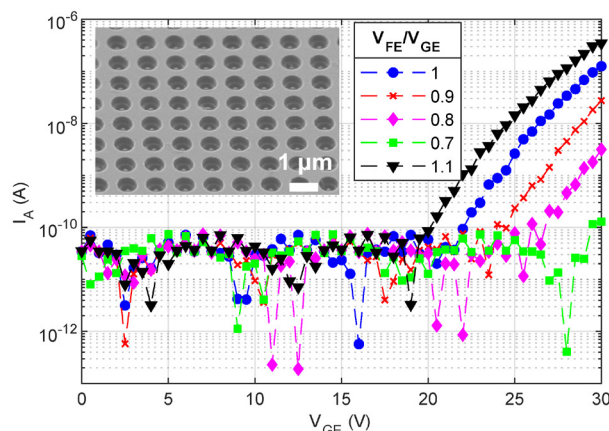
The advent of microfabrication has enabled scalable and high-density Si field-emitter arrays (FEAs). These are advantageous due to compatibility with complementary metal-oxide-semiconductor (CMOS) processes, the maturity of the technology, and the ease in fabricating sharp tips using oxidation. The use of a current limiter is necessary to avoid burn-out of the sharper tips. Active methods using integrated MOS field-effect transistors and passive methods using a nano-pillar (~200-nm wide, 8- μm tall) in conjunction with the tip have been demonstrated. Si FEAs with single gates reported in our previous works have current densities of >100 A/cm² and operate with lifetimes of over 100 hours.

The need for another gate (Figure 1) becomes essential to control the focal spot size of the electron beam as electrons leaving the tip have an emission angle of 12.5°. The focus electrode provides a radial electric field that reduces the lateral velocity of stray electrons

and narrows the cone angle of the beam reaching the anode. Varying the voltage on the focus gate reduces the focal spot size or achieves an electron beam modulator for radio-frequency applications. In this work, we fabricate the densest (1- μm pitch) double-gated Si with an integrated nanowire current limiter (Figure 2). The apertures are ~350 nm and ~550 nm for the extractor and focus gates, respectively, with a 350-nm-thick oxide insulator separating the two gates. Electrical characterization of the fabricated devices shows that the focus-to-gate ratio (V_{FE}/V_{GE}) can be used to control the anode current (Figure 2). When the focus voltage exceeds the gate voltage, the field superposition increases the extracted current, and vice versa. These devices can potentially find applications as high-current focused electron sources in flat panel displays, nano-focused X-ray generation, and microwave tubes.



▲ Figure 1: Si field-emitter array with integrated current limiter, self-aligned extractor, and focus gates for nano-focused cold electron sources.



▲ Figure 2: Electrical characterization of 500 x 500 arrays with different focus/gate voltage ratios; inset shows the fabricated double-gated array.

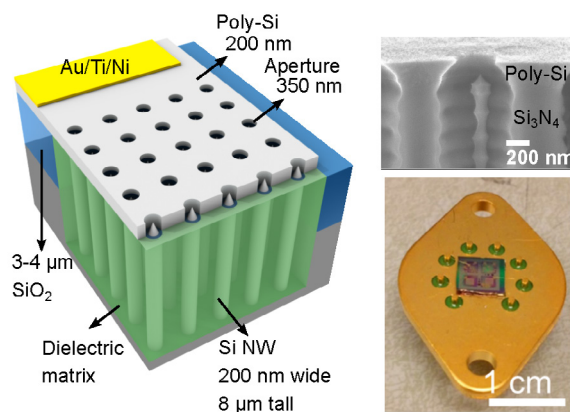
FURTHER READING

- G. Rughoobur, N. Karaulac, L. Jain, O. O. Omotunde, and A. I. Akinwande, "Nanoscale Silicon Field Emitter Arrays with Self-aligned Extractor and Focus Gates," *Nanotechnology*, vol. 31, no. 33, p. 335203, 2020.
- L. Y. Chen and A. I. Akinwande, "Aperture-collimated Double-gated Silicon Field Emitter Arrays," *IEEE Trans. Electron Devices*, vol. 54, no. 3, pp. 601–608, 2007.
- L. Dvorson, I. Kymissis, and A. I. Akinwande, "Double-gated Silicon Field Emitters," *J. Vac. Sci. Technol. B Microelectron. Nanom. Struct.*, vol. 21, no. 1, p. 486, 2003.

Gated Silicon Field-Ionization Arrays for Compact Neutron Sources

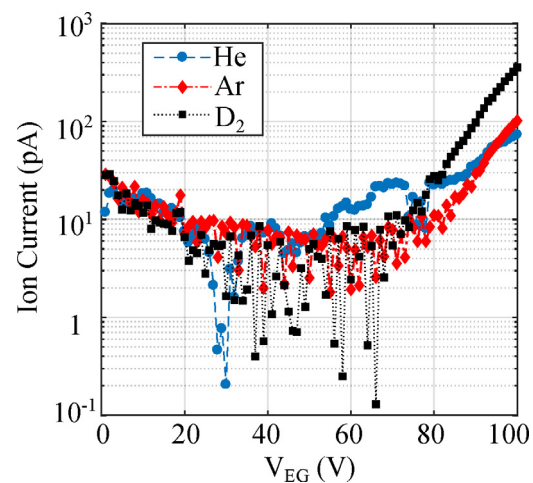
G. Rughoobur, A. I. Akinwande
Sponsorship: DARPA

Neutron radiation is widely used in various applications, ranging from the analysis of the composition and structure of materials and cancer therapy to neutron imaging for security. However, most applications require a large neutron flux, which is often achieved only in large infrastructures such as nuclear reactors and accelerators. Neutrons are generated by ionizing deuterium (D_2) to produce deuterium ions (D^+) that can be accelerated towards a target loaded with either D or tritium (T). The reaction generates neutrons and isotopes of He, with the D-T reaction producing the higher neutron yield. Classic ion sources require extremely high positive electric fields, on the order of 10^8 volts per centimeter (10 V/nm). Such a field is achievable only in the vicinity of sharp electrodes under a large bias; consequently, ion sources for neutron generation are bulky.



▲ Figure 1: Schematic of gated field-ionization array, with SEM cross section of a single field ionizer and photograph of a packaged chip with arrays of different sizes for neutron generation.

This work explores, as an alternative, highly scalable and compact Si field-ionization arrays (FIAs) with a unique device architecture that uses self-aligned gates and a high-aspect-ratio (~40:1) Si nanowire current limiter to regulate electron flow to each field emitter tip in the array (Figure 1). The tip radius has a log-normal distribution with a mean of 5 nm and a standard deviation of 1.5 nm, while the gate aperture is ~350 nm in diameter and is within 200 nm of the tip. Field factors, β , of $> 1 \times 10^6 \text{ cm}^{-1}$ can be achieved with these Si FIAs, implying that gate-emitter voltages of 250-300 V (if not less) can produce D^+ based on the tip field of 25-30 V/nm. In this work, our devices achieve an ionization current of up to 5 nA at ~140 V for D_2 at pressures of 10 mTorr. Gases such as He and Ar can also be ionized at voltages (<100 V) with these compact Si FIAs (Figure 2).



▲ Figure 2: Ion current measured for different gases (He, Ar, and D_2) at 1 mTorr pressure demonstrating low ionization voltages using 1000 by 1000 Si FIAs.

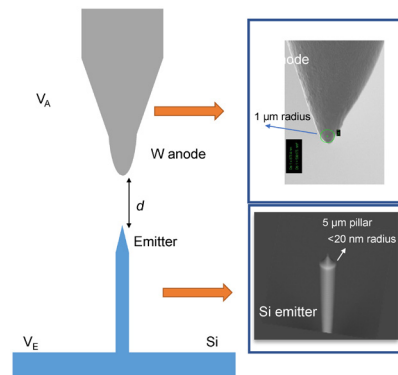
FURTHER READING

- A. Fomani, L. F. Velasquez-Garcia, and A. I. Akinwande, "Low-voltage Field Ionization of Gases up to Torr-level Pressures using Massive Arrays of Self-aligned Gated Nanoscale Tips," *IEEE Trans. Electron Devices*, vol. 61, no. 5, pp. 1520–1528, 2014.
- G. Rughoobur, A. Sahagun, O. O. Ilori, and A. I. Akinwande, "Nanofabricated Low-Voltage Gated Si Field-Ionization Arrays," *IEEE Trans. Electron Devices*, vol. 1, no. c, pp. 1–7, 2020.
- B. Johnson, P. R. Schwoebel, P. J. Resnick, C. E. Holland, K. L. Hertz, and D. L. Chichester, "Field Ionization Characteristics of an Ion Source Array for Neutron Generators," *J. Appl. Phys.*, vol. 114, no. 17, p. 174906, Nov. 2013.

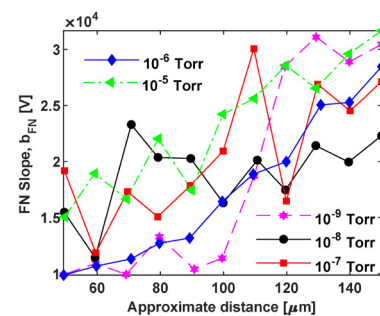
Field Emission from a Single Nanotip in Controlled Poor Vacuum

G. Rughoobur, O. O. Ilori, A. I. Akinwande
Sponsorship: DARPA

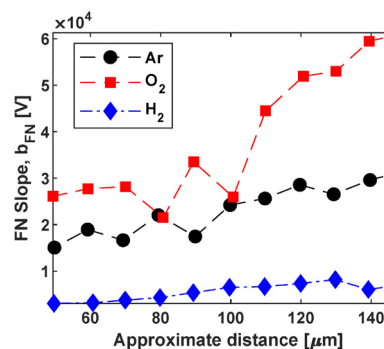
For reliable field emission performance, nano-emitters require ultra-high vacuum, which is bulky and costly. In poor vacuum, the adsorption/desorption of gas molecules on the surface causes work function variations, which results in exponential changes in the emitted current. In this work, we assess the dependence of the Fowler-Nordheim slope, b_{FN} , in different gases using a single un-gated Si emitter. These measurements are enabled by using a scanning anode field emission microscope that has a W tip (radius $<1\ \mu\text{m}$) as the anode and with the Si emitter placed on a nano-positioning stage. We first characterized the devices in ultra-high vacuum and in the following gases: Ar, He, N_2 , O_2 , and H_2 . I-V characteristics are recorded by varying the distance, d , between the anode and the emitter (Figure 1). Using the measurement in ultra-high vacuum (UHV, 10^{-9} Torr) as a reference, we extract the geometrical field-factor, β from b_{FN} . In poor-vacuum measurements (10^{-8} Torr – 10^{-5} Torr), we use this β to extract the “modified” work-function of the surface for each gas and each pressure investigated. We find that as pressure increases, the performance in Ar changes very little at the distances scanned (Figure 2). As expected (Figure 3), operation in O_2 resulted in substantial increase in b_{FN} and hence the work-function; however, in H_2 , we measured a decrease in the slope, suggesting a reduction in the work function. This work provides the premise in assessing which gases and pressures are responsible for performance degradation in Si field-emitter arrays, to achieve more stable field-emission current in poor vacuum.



▲ Figure 1: Schematic of measurement of a single Si emitter using a scanning anode field emission microscope using a W anode positioned at a distance d . Scanning electron microscope images of the emitter and the anode.



▲ Figure 2: FN slope extracted for UHV with decreasing d , compared with different pressures of Ar showing only a small increase in b_{FN} .



▲ Figure 3: Comparison of different gases on the FN slope at 10^{-5} Torr demonstrating larger b_{FN} in O_2 , and smaller b_{FN} in H_2 .

FURTHER READING

- G. Rughoobur, J. Zhao, L. Jain, A. Zubair, T. Palacios, J. Kong, and A. I. Akinwande, “Enabling Atmospheric Operation of Nanoscale Vacuum Channel Transistors,” *2020 Device Research Conference (DRC)*, 2020, pp. 1–2.
- L. F. Velásquez-García, S. A. Guerrero, Y. Niu, and A. I. Akinwande, “Uniform High-Current Cathodes Using Massive Arrays of Si Field Emitters Individually Controlled by Vertical Si Ungated FETs-Part 2: Device Fabrication and Characterization,” *IEEE Trans. Electron Devices*, vol. 58, no. 6, pp. 1783–1791, Jun. 2011.
- P. R. Schwoebel and I. Brodie, “Surface-science aspects of vacuum microelectronics,” *J. Vac. Sci. Technol. B Microelectron. Nanom. Struct.*, vol. 13, no. 4, pp. 1391–1410, 1995.

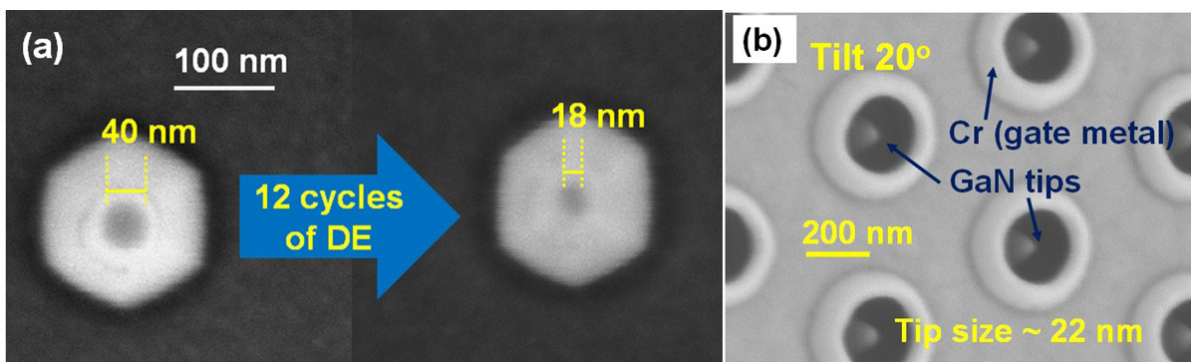
GaN Vertical Nanostructures Sharpened by A New Digital Etching Process for Field Emission Applications

P.-C. Shih, T. Palacios, in collaboration with G. Rughoobur, A. I. Akinwande
Sponsorship: AFOSR

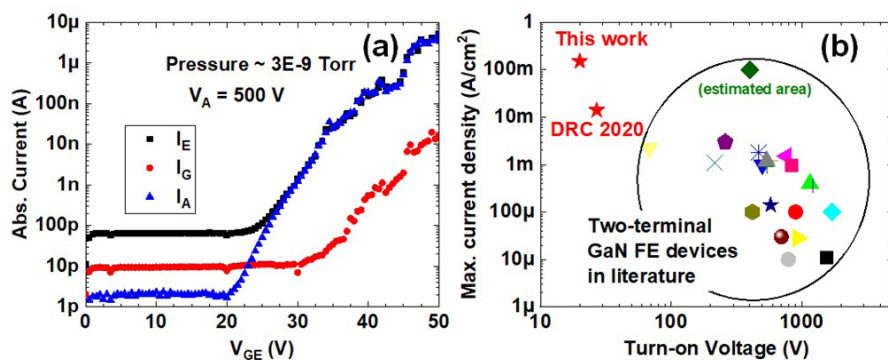
Field emitters (FE), namely vacuum transistors, are promising for harsh-environments and high-frequency electronics. III-nitrides are excellent candidates as FEs due to their tunable electron affinities. However, so far, few works demonstrate sub-100 V turn on in III-nitride field emission devices because of relatively large tip sizes and the lack of self-aligned gate structures.

In this work, we develop a novel wet-based-only digital etching (DE) process for GaN nanopyramid field emission arrays (FEAs). Conventional oxygen-plasma-based DEs on III-nitrides are anisotropic, and they do not sharpen vertical tips. Furthermore, the use of a biased plasma could potentially damage tips. Therefore, a new digital etching process is developed. By using this new technology, tip width can be sharpened from 40 nm down to sub-20 nm with a reasonably controlled etching rate per cycle of DE (Figure 1 (a)).

Combining the sharpened GaN nanopyramids with a self-aligned-gate structure (Figure 1 (b)) we developed before, we demonstrate the world's-best GaN vertical field emission devices with the lowest gate-emitter turn-on voltage ($V_{GE, ON}$) of 20 V and the highest max current density of 150 mA/cm² at $V_{GE} = 50$ V (Figure 2). The turn-on voltage and field factor of this device are also already comparable with the-state-of-art Si FEAs. Furthermore, the gate leakage is still only about 0.5 % of the anode current, indicating a space to have future improvement for more drive current. Further performance improvements are expected when applying the developed technologies to N-polar III-nitrides and AlGaIn-alloys.



▲ Figure 1: Scanning electron microscope images of (a) a tip before and after DE and (b) finished device.



▲ Figure 2: (a) Transfer characteristics of this gated GaN vertical FEA and (b) benchmark of GaN vertical FEs.

FURTHER READING

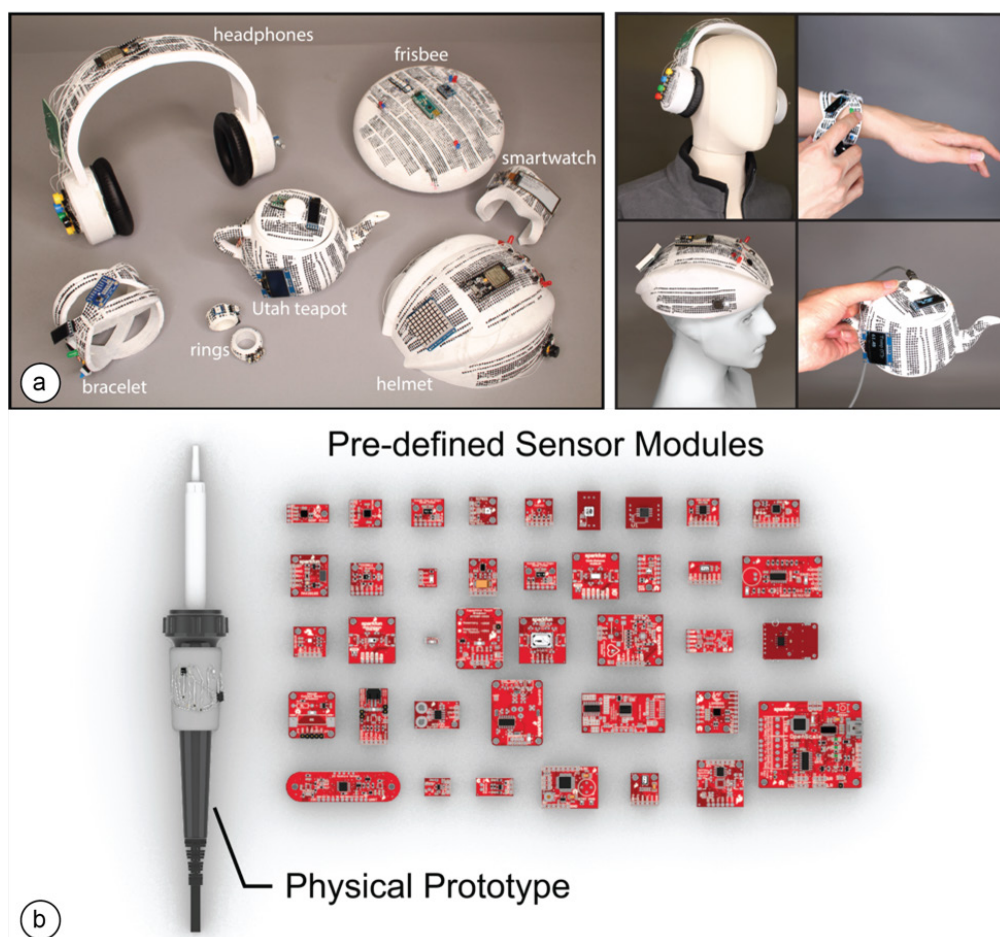
- P.-C. Shih, G. Rughoobur, K. Cheng, A. I. Akinwande, and T. Palacios, "Self-Align-Gated GaN Field Emitter Arrays Sharpened by a Digital Etching Process," *IEEE Electron Device Letters*, vol. 42, no. 3, Mar. 2021, pp. 422-425.
- P.-C. Shih, G. Rughoobur, P. Xiang, K. Liu, K. Cheng, A. I. Akinwande, and T. Palacios, "GaN Nanowire Field Emitters with a Self-Aligned Gate Process," presented at *78th Device Research Conference*, virtual, Jun. 2020.

Integrating Object Form and Electronic Function in Rapid Prototyping and Personal Fabrication

J. Zhu, S. Mueller
Sponsorship: NSF, NCSOFT

Rapid prototyping is a key technique that enables users to quickly realize their digital designs and therefore has been widely used in early-stage prototyping and small-scale customized fabrication. A long-term vision in human-computer interaction is to create interactive objects for which all functions are directly integrated with the form and fabricated at once. So far, rapid prototyping has focused mainly on fabricating passive objects for which the form of an object can be freely

designed; recently we have also moved towards digital specification and fabrication of object functions for interactive design. These advances offer the promise that eventually in rapid function prototyping, the interactive object form and function would be under the same design consideration; therefore, the object form could follow its designated function, and the function could adapt to its physical form.



▲ Figure 1: (a) CurveBoards are 3D breadboards directly integrated into the surface of physical objects. (b) MorphSensor is a 3D electronics design tool for designing electronic function in the context of a prototype's three-dimensional shape.

FUTURE READING

- J. Zhu, L. Blumberg, Y. Zhu, M. Nisser, E. L. Carlson, X. Wen, K. Shum, J. A. Quaye, and S. Mueller, "CurveBoards: Integrating Breadboards into Physical Objects to Prototype Function in the Context of Form," in *Proceedings of the 2020 CHI Conference on Human Factors in Computing Systems (CHI '20)*, ACM, 2020.
- J. Zhu, Y. Zhu, J. Cui, L. Cheng, J. Snowden, M. Chounlakone, M. Wessely and S. Mueller, "MorphSensor: A 3D Electronic Design Tool for Reforming Sensor Modules," in *Proceedings of the 33rd Annual ACM Symposium on User Interface Software and Technology (UIST '20)*, ACM, 2020.

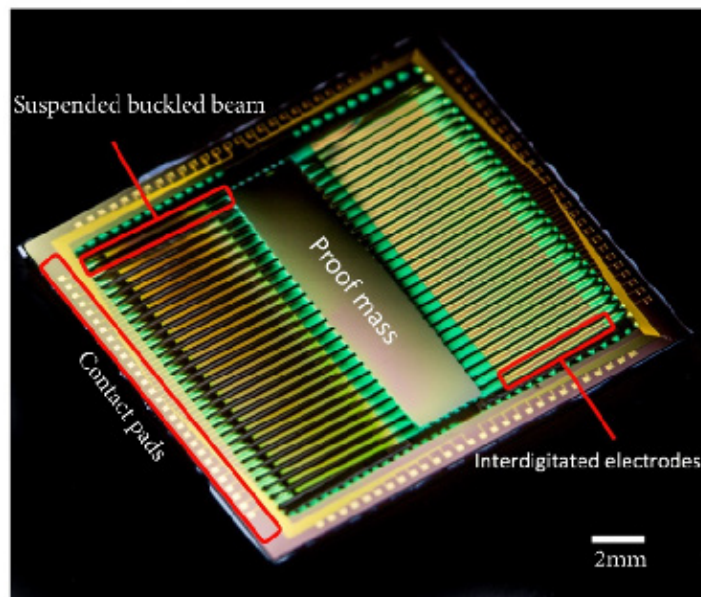
MEMS Energy Harvesting and AI-based Design Processing

H. Akay, S-G. Kim

Sponsorship: MIT-SUTD International Design Center

Vibrational energy-harvesting devices seek to deliver useable electric power in remote or mobile applications by drawing energy from ambient sources of vibration. Due to the spectrum of such ambient vibrations occurring at a very low frequency (below 100Hz), major design challenges must be overcome when developing a piezoelectric energy harvesting device to function in these conditions, namely generating strain at the micro-scale and operating over a wide bandwidth of low input frequencies. The culmination of three generations of this microelectromechanical systems (MEMS) design effort by our research group is a bi-stable buckled beam energy harvester that relies on non-linear oscillations to translate input vibrations to the axial strain of piezoelectric elements to produce sizable electric energy at the MEMS-scale devices.

Various long-term research efforts such as this at MIT produce documentation detailing novel devices and corresponding process designs that could benefit future micro and nano systems designers if the knowledge and design concepts explored for them could be computationally retrievable. To benefit from past designs, their functional requirements must be identified and structured in a searchable and trainable knowledge base which future designers may navigate. Currently, we are developing an AI-based Natural Language Processing (NLP) model which can automate the reading of vast MEMS documentation produced by MTL and MIT.nano. By automatically processing and representing decades of research knowledge at MIT and elsewhere, faster and successful design and innovation in MEMS and Nano-scale systems can be achieved.



▲ Figure: Photograph of fabricated bi-stable buckled beam energy-harvesting device.

FURTHER READING:

- R. Xu, H. Akay & S.G. Kim, "Buckled MEMS Beams for Energy Harvesting from Low Frequency Vibrations," Research, 2019.
- H. Akay, M. Yang & S.G. Kim, "Automating Design Requirement Extraction from Text with Deep Learning," *ASME IDETC/CIE Design Automation Conference*, 2021.
- H. Akay & S.G. Kim, "Reading Functional Requirements Using Machine Learning-based Language Processing," *CIRP Annals* 70(1), 2021.

Nanotechnology, Nanostructures, Nanomaterials

Lithiation Mechanisms of Si and Ge Thin Film Battery Electrodes.....	93
Gated Nonreciprocal Magnon Transmission from Direction-Dependent Magnetic Damping.....	94
Gigahertz Frequency Antiferromagnetic Resonance and Strong Magnon-Magnon Coupling in Layered Crystal CrCl ₃	95
Nanoparticle-Enhanced Microsputtered Gold Thin Films for Low-Cost, Agile Manufacturing of Interconnects.....	96
Large-Scale 2D Perovskite/Transition Metal Dichalcogenide Heterostructure for Photodetector.....	97
Grayscale Stencil Lithography.....	98
Unraveling the Correlation between Raman and Photoluminescence in Monolayer Molybdenum Disulfide through Machine Learning Models.....	99
Additively Manufactured Electro spray Ion Thrusters for Cubesats.....	100
Low-Temperature Growth of High Quality MoS ₂ by Metal-Organic Chemical Vapor Deposition.....	101
Self-Assembly via Defect-Mediated Metal Nanoisland Nucleation on 2D Materials.....	102
Strain Control of Nanocatalyst Synthesis.....	103
Controlled Cracking to Improve Mechanical Stability of RuO ₂ Thin-Film Li-ion Electrodes.....	104
Seeing Superlattices: Imaging Moiré Periods at the Nanoisland-2D Material Interface Using Scanning Transmission Electron Microscopy.....	105
Small-Molecule Assemblies Inspired by Kevlar: Aramid Amphiphile Nanoribbons.....	106

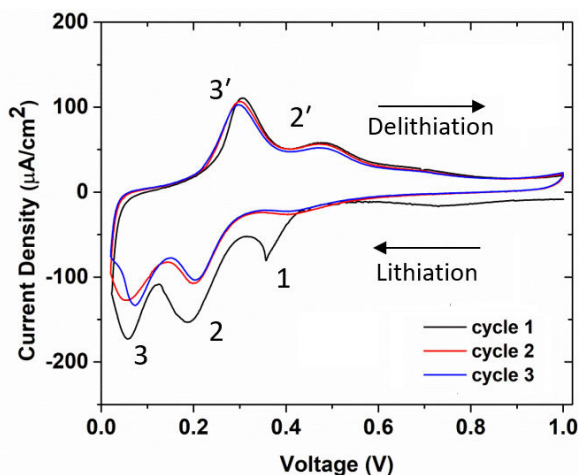
Lithiation Mechanisms of Si and Ge Thin Film Battery Electrodes

J. Miao, B. Wang, C. V. Thompson

Sponsorship: Skolkovo Institute of Science and Technology, SMART

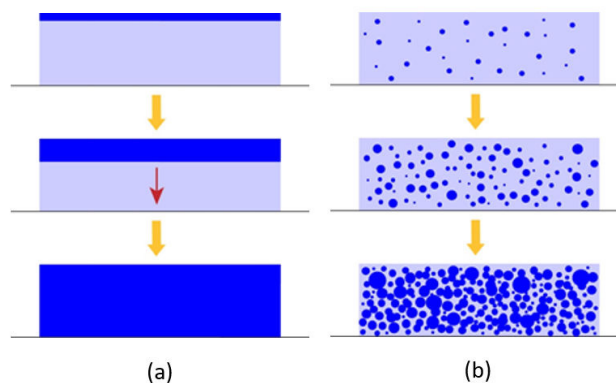
Thin film batteries (TFBs) made using complementary metal-oxide-semiconductor- (CMOS) compatible materials and processes can be integrated with CMOS circuits and energy harvesting and sensing devices to produce low-cost autonomous sensors with small form factors. As part of our research on CMOS-compatible Li-ion TFBs, we are studying Si and Ge films to be used as anode electrodes. While these materials have the highest known charge capacity (8300 mA/cm³ for Si and 7300 mA/cm³ for Ge), they tend to have poor reliability (low cyclability) due to mechanical failures associated with large volume changes. The mechanisms through which lithium is stored in these materials are also poorly understood but are known to be related to poor cyclability. We have carried out mechanistic studies of reversible lithium storage in Si and Ge films using both electrochemical and physical characterization techniques.

Figure 1 shows current-voltage measurements made during the first three lithiation/delithiation cycles of a 315-nm-thick amorphous Si film (a cyclic voltammogram, CV). The current corresponds



▲ Figure 1: CV for the first three cycles of a 315-nm-thick amorphous Si thin film. The current density is related to insertion of Li into Si during lithiation and removal of Li during delithiation. Peaks correspond to phase transitions.

to Li being stored in the electrode (lithiation) or removed (delithiation). Peaks in these curves indicate accelerated charging or discharging associated with phase transitions, all of which are between amorphous phases with different stoichiometries (increasingly Li-rich for lithiation). An irreversible transition is seen in the first cycle (peak 1 in Figure 1), and two reversible transitions are seen in all three and all subsequent cycles (peaks 2-2' and 3-3'). Through new potentiostatic and transmission electron microscopy techniques, we have established that the irreversible transition occurs through propagation of a reaction through the thickness of the film (Figure 2b) and that the reversible transitions occur through an amorphous-to-amorphous nucleation and growth process (Figure 2b), sometimes referred to as a polyamorphous phase transition. In similar experiments on Ge, we have focused on the reversible transition of a Li-rich amorphous phase to a crystalline phase, which also occurs through a nucleation and growth process. These studies have been correlated with the reliability of TFBs.



▲ Figure 2: Schematic illustrations of cross sections of Si films during phase transitions associated with peaks in Figure 1. (a) Irreversible propagation of a sharp interface between two amorphous phases (peak 1). (b) Reversible nucleation and growth transitions between two amorphous phases (peaks 2-2' and 3-3').

FURTHER READING

- J. Miao and C. V. Thompson, "Kinetic Study of the Initial Lithiation of Amorphous Silicon Thin Film Anodes," *J. Electrochem. Soc.*, vol. 165, pp. A650-A656, 2018.
- J. Miao, B. Wang, and C. V. Thompson, "First-order Amorphous-to-Amorphous Phase Transitions During Lithiation of Silicon Thin Films," *Phys. Rev. Materials*, vol. 4, p. 043608, 2020.
- J. Miao, B. Wang, and C. V. Thompson, "Kinetic Study of Lithiation-induced Phase Transitions in Amorphous Germanium Thin Films," *J. Electrochem. Soc.*, vol. 167, p. 090557, 2020.

Gated Nonreciprocal Magnon Transmission from Direction-Dependent Magnetic Damping

J. Han, Y. Fan, B. C. McGoldrick, J. Finley, J. T. Hou, P. Zhang, L. Liu
Sponsorship: NSF, SRC

An important application of magnetic materials in information technology is to provide nonreciprocity, which allows unidirectional signal transmission. A representative device is the two-terminal microwave isolator. A ferromagnet inside naturally breaks the time-reversal symmetry and allows microwave transmission only from port 1 to port 2, while signals from port 2 to port 1 are suppressed. Despite wide applications, these conventional nonreciprocal devices suffer from their bulk volume and the difficulty of being integrated into high-density circuits. Nowadays, new mechanisms that can provide passive and directional isolation of signals are being pursued at sub-micrometer scale. Among various proposals, magnons, the quanta of the collective excitation of magnetic moments, show unique potential due to the tunability and the possibility for on-chip integration. So far, nonreciprocal magnon transmission has been achieved only at resonant conditions with

gigahertz frequency. It is unclear if nonreciprocity can still be observed for magnons with a broad spectrum up to terahertz frequency.

Here we show that using a magnetic gate, one can realize tunable nonreciprocal propagation in spin Hall effect-excited incoherent magnons, whose frequency covers the spectrum from a few gigahertz up to terahertz. We further identify the direction-dependent magnetic damping as the dominant mechanism for the nonreciprocity, which originates from the interlayer dipolar coupling and works both in the ballistic and diffusive regions of magnons. As a natural result of the chiral magnon-magnon coupling, our findings provide a general mechanism for introducing directional magnon transmission and lead to a design of passively gated magnon transistors for applications of information transmission and processing.

Gigahertz Frequency Antiferromagnetic Resonance and Strong Magnon-Magnon Coupling in Layered Crystal CrCl_3

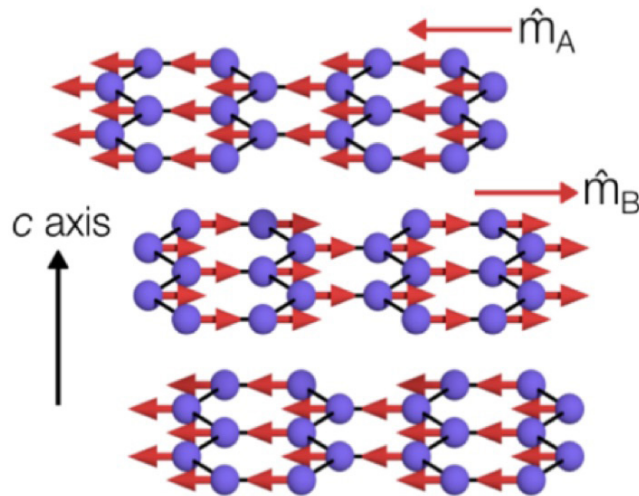
J. T. Hou, D. MacNeill, D. R. Klein, P. Zhang, P. Jarillo-Herrero, L. Liu

Sponsorship: DoE Office of Science, Gordon and Betty Moore Foundation, NSF, NSF GRFP

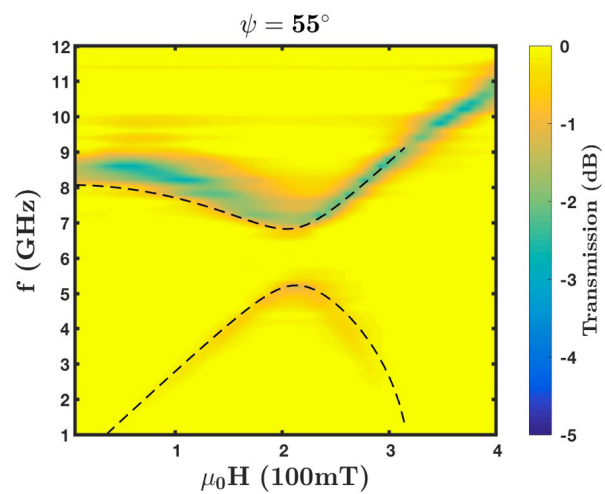
Magnon-magnon hybrid systems have recently been realized between two adjacent magnetic layers, with potential applications to hybrid quantum systems and coherent information processing. Realizing magnon-magnon coupling within a single material requires antiferromagnetic (AFM) or ferrimagnetic materials with magnetic sublattice structures. However, conventional AFM resonance lies in terahertz frequencies, which require specialized techniques to probe.

In this work, we realize strong magnon-magnon coupling within a single material, CrCl_3 . CrCl_3 is a layered van der Waals AFM material, with parallel intralayer alignment and antiparallel interlayer alignment of magnetic moments (Figure 1). Because of weak anisotropy and interlayer magnetic coupling,

we observe both optical and acoustic modes of AFM resonances within the range of typical microwave electronics ($<20\text{GHz}$), in contrast to conventional AFM resonances. By breaking rotational symmetry, we further show that strong magnon-magnon coupling with large tunable gaps can be realized between the two resonant modes (Figure 2). Our results demonstrate strong magnon-magnon coupling within a single material and establish CrCl_3 as a convenient platform for studying AFM dynamics in microwave frequencies. Because CrCl_3 is a van der Waals material that can be cleaved to produce air-stable monolayer thin films, these results open up the possibility to realize magnon-magnon coupling in magnetic van der Waals heterostructures by symmetry engineering.



▲ Figure 1: Magnetic structure of bulk CrCl_3 below the Neel temperature. Blue spheres represent Cr atoms.



▲ Figure 2: Strong magnon-magnon coupling realized with magnetic field applied at a 55° angle with respect to the crystal plane.

FURTHER READING

- D. MacNeill, J. T. Hou, D. R. Klein, P. Zhang, P. Jarillo-Herrero, and L. Liu, *Physical Review Letters*, vol. 123, p. 047204, 2019.

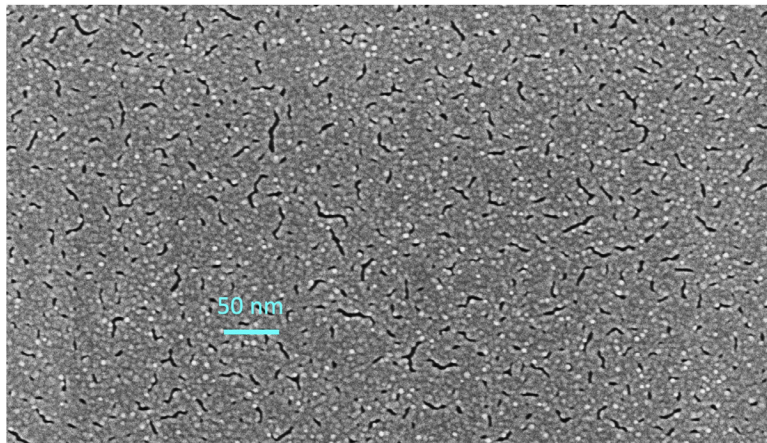
Nanoparticle-Enhanced Microsputtered Gold Thin Films for Low-Cost, Agile Manufacturing of Interconnects

Y. Kornbluth, R. Mathews, L. Paramswaran, L. Racz, L.F. Velásquez-García
Sponsorship: US Air Force

Silicon and gold are ubiquitous in the microelectronics industry—silicon as the cornerstone of semiconductor devices, and gold as a material with unmatched electro-optical properties. However, gold films do not adhere well to silicon or silicon dioxide, necessitating the need for an adhesion layer made of a third material. This need increases complexity and cost. Also, reworking interconnects via traditional (cleanroom) technology poses challenges, e.g., thermal budget, vacuum compatibility.

In this project, we explore microplasma sputtering to implement at low-cost interconnects for agile electronics. We have shown that under proper operational conditions, a microplasma sputterer creates at room temperature and atmospheric pressure dense, highly conductive gold films with a fivefold better adhesion than the state of the art, without using an adhesion layer, annealing, or any other pre/post printing steps. If the gold film is sputtered in an

atmospheric-pressure microsputterer in the presence of a fast-moving jet of air, gold nanoparticles form. The high collisionality of the atmospheric-pressure gas and high energy of the plasma facilitate nanoparticle formation, while the jet carries the nanoparticles to the substrate. The speed of the jet of air determines the size of the nanoparticles. These nanoparticles then act as an adhesion layer to allow a gold film, made of these nanoparticles and individual atoms, to adhere well to a silicon or silicon dioxide substrate. By rastering the printhead over the desired deposition area, we can interweave large nanoparticles and smaller atoms, creating a dense film (Figure 1). This process allows us to optimize adhesion, density, and conductivity simultaneously. Conductivity of the resultant films is also near-bulk (120% of bulk gold—the highest value reported for a room-temperature additive manufacturing method), allowing for their use in microelectronics.



▲ Figure 1: SEM micrograph of microsputtered gold imprint (from Kornbluth et al., *Additive Manufacturing*, vol. 36, p. 101679, Dec. 2020). The film is dense, highly electrically conductive and is made of the agglomeration of nanoparticles created in the plume of a room-temperature, atmospheric pressure microsputterer.

FURTHER READING

- Y. Kornbluth, R. H. Mathews, L. Parameswaran, L. M. Racz, and L. F. Velásquez-García, "Nano-additively Manufactured Gold Thin Films with High Adhesion and Near-bulk Electrical Resistivity via Jet-assisted Nanoparticle-dominated, Room-temperature Microsputtering," *Additive Manufacturing*, vol. 36, p. 101679, Dec. 2020.
- Y. Kornbluth, R. H. Mathews, L. Parameswaran, L. M. Racz, and L. F. Velásquez-García, "Room-temperature, Atmospheric-pressure Microsputtering of Dense, Electrically Conductive, Sub-100 nm Gold Films," *Nanotechnology*, vol. 30, no. 28, p. 285602, Apr. 2019.
- Y. Kornbluth, R. H. Mathews, L. Parameswaran, L. M. Racz, and L. F. Velásquez-García, "Microsputterer with Integrated Ion-drag Focusing for Additive Manufacturing of Thin, Narrow Conductive Lines," *Journal of Physics D – Applied Physics*, vol. 51, no. 16, p. 165603, Apr. 2018.

Large-Scale 2D Perovskite/Transition Metal Dichalcogenide Heterostructure for Photodetector

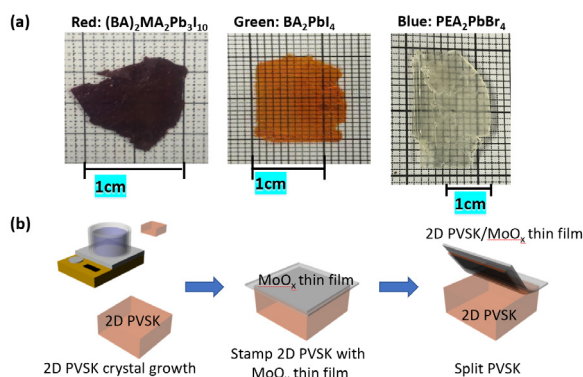
D. Lee, S. Bae, J. Kim
Sponsorship: SUSTECH

Monolayer transition metal dichalcogenides (TMDCs) have been attractive nanomaterials for optoelectronics due to their extremely high quantum efficiency, but their atomically thin thickness prevents them from absorbing sufficient light for optoelectrical applications.

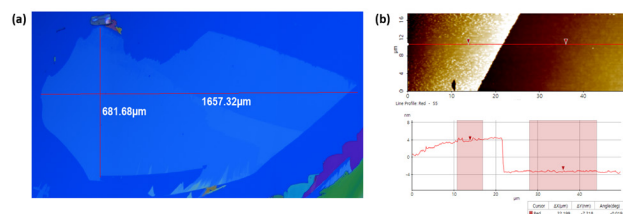
To improve the optoelectrical performance of TMDCs, during the past years, 2D Ruddlesden-Popper perovskites (PVSs)/TMDC heterostructures have been demonstrated. Thanks to their high absorption coefficient, long diffusion length of charge carrier, sharp exciton emission, and high power conversion efficiency, 2D PVSs have been used as an absorption layer for TMDCs. However, 2D PVS/TMDC heterostructures are limited in the micrometer scale,

since 2D PVSs have been fabricated only by the tape-exfoliation method.

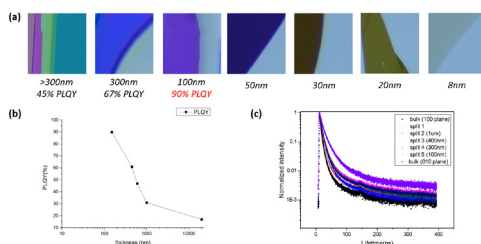
We reported a layer resolved splitting (LRS) technique to isolate multilayer 2D materials into a monolayer in wafer scale in 2018. To improve the scalability of 2D PVSs for large-scale application, in this work, we successfully split micrometer-thick 2D PVSs into nanometer-thick and millimeter-width scale with the LRS technique. We also obtained 90% of photoluminescence quantum yield, which is the world's best record to the best our knowledge. Then we plan to demonstrate large-scale 2D PVS/TMDC heterostructures for photodetectors, which only has been previously demonstrated up to micrometer scale.



▲ Figure 1: (a) Images of as-grown bulk 2D perovskite single crystals (b) schematic of stamping process to split 2D perovskite into atomic layer



▲ Figure 2: (a) Optical image of 8nm-thick and mm-width scale 2D perovskite layers (b) AFM image of split 2D perovskite layer.



▲ Figure 3: (a) Optical images of split 2D perovskite layers with different thickness (b) Photoluminescence quantum yield (PLQY) of 2D perovskite with different thickness (c) Carrier lifetime of 2D perovskite with different thickness.

FURTHER READING

- J. Shim, et al., "Controlled Crack Propagation for Atomic Precision Handling of Wafer-scale Two-dimensional Materials," *Science*, vol. 362, pp. 665-670, 2018.
- U. Erkiş, et al., "Vapor Phase Selective Growth of Two-dimensional Perovskite/WS₂ Heterostructures for Optoelectronic Applications," *ACS Applied Materials & Interfaces*, vol. 11, no. 43, pp. 40503-40511, 2019.
- Q. Wang, et al., "Optoelectronic Properties of a van der Waals WS₂ Monolayer/2D Perovskite Vertical Heterostructure," *ACS Applied Materials & Interfaces*, vol. 12, no. 40, pp. 45235-45242, 2020.

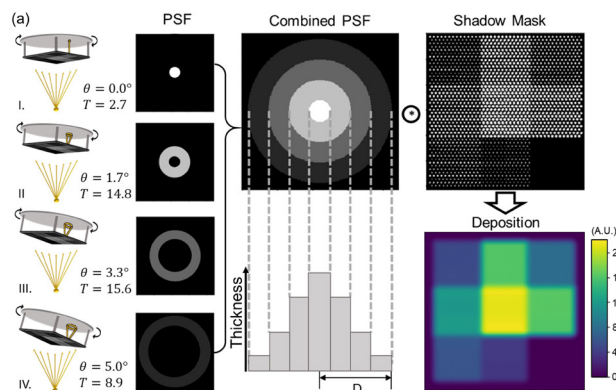
Grayscale Stencil Lithography

X. H. Li, Z. J. Tan, N. Fang
Sponsorship: ExxonMobil

In this work, we demonstrate a new eBeam evaporation method with fixed single stencil shadow mask to generate 2D patterns with spatial thickness variation across wafer-scale substrate. This method outperforms conventional approaches like the iterative photo-lithography-and-lift-off method or grayscale photolithography, due to their limitations of efficiency, material choices, and manufacturing complexity. We applied the method to create a multi-spectral reflective color filter arrays with two layers of variable thickness. It offers a broader design space to achieve a wide color spectrum with simple and efficient fabrication procedures. This method shows potential for scaling up and high-resolution patterning, which could be widely applied in manufacturing for optical imaging, sensing, and computing.

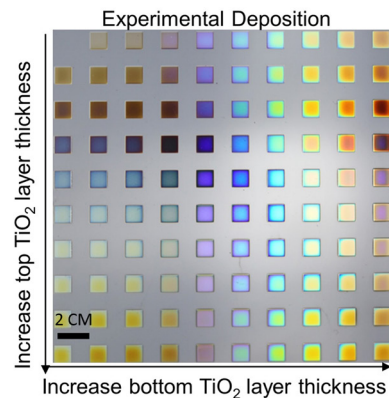
The method takes inspiration from the “pin-hole imaging” in optics to generate the convoluted pattern of the material source and the stencil shadow mask, as shown in Figure 1.

The ejection of materials in the eBeam pockets is analogous to the “light source,” which passes through the pin holes on the shadow masks to finally cast the “image” in terms of deposition thickness. By controlling the deposition dose (T) and the tilting angle (θ) of the substrate, we could create the “point spreading function” (PSF) of the material target passing through the shadow mask, which can create smooth deposition with less than 5-nm surface roughness. As shown in Figure 2, we applied this method to create a multi-spectral color filter array and a 2D pattern of the MIT “Dome” to demonstrate the capability of this method for customizable patterning. Higher resolution deposition is also possible by combining the available micro/nano stencil lithography techniques and our grayscale stencil lithography method.



▲ Figure 1: Schematic of PSF control and convoluted deposition of the grayscale stencil lithography method.

► Figure 2: Demonstration of spatially variable thickness deposition for multispectral color filter array and MIT “Dome.”



FURTHER READING

- X. H. Li, Z. J. Tan, and N. Fang, “Grayscale Stencil Lithography for Patterning Multispectral Color Filters,” *Optica*, vol. 7, no. 9, pp. 1154–1161, Sep. 2020.
- K. Du, J. Ding, Y. Liu, I. Wathuthanthri, and C.H. Choi, “Stencil Lithography for Scalable Micro and Nano Manufacturing,” *Micromachines*, vol 8, no. 4, pp. 131–155, Apr. 2017.

Unraveling the Correlation between Raman and Photoluminescence in Monolayer Molybdenum Disulfide through Machine Learning Models

A.-Y. Lu, L. G. Pimenta-Martins, P.-C. Shen, J.-H. Park, Z. Chen, J. Han, J. Kong
Sponsorship: ISN

Two-dimensional (2D) transition metal dichalcogenides (TMDs) with intense and tunable photoluminescence (PL) have opened up new opportunities for optoelectronic and photonic applications such as light-emitting diodes, photodetectors, and single-photon emitters. Among the standard characterization tools for 2D materials, Raman spectroscopy stands out as a fast and non-destructive technique capable of probing materials' crystallinity and perturbations such as doping and strain. However, the correlation between photoluminescence and Raman spectra in monolayer MoS₂ remains elusive due to its highly nonlinear correlation. Here, we systematically explore the correlation between PL signatures and Raman modes through ma-

chine learning models. First, we adopt a convolution neural network, DenseNet, to predict PL by spatial Raman maps with relatively small pixel dimensions but deep channels. Moreover, we apply a gradient boosted trees model (XGBoost) with the Shapley additive explanation (SHAP) to evaluate the impact of individual Raman features in PL behavior, which allows us to further link the strain and doping of monolayer MoS₂ with its PL behavior. Our analytical method unravels the nonlinear correlations of physical or chemical properties for 2D materials and provides the knowledge for tuning and synthesizing 2D semiconductors for high-yield photoluminescence.

FURTHER READING

- Y. Kornbluth, R. H. Mathews, L. Parameswaran, L. M. Racz, and L. F. Velásquez-García, "Room-temperature, Atmospheric-pressure Microsputtering of Dense, Electrically Conductive, Sub-100 nm Gold Films," *Nanotechnology*, vol. 30, no. 28, p. 285602, Apr. 2019.
- Y. Kornbluth, R. H. Mathews, L. Parameswaran, L. M. Racz, and L. F. Velásquez-García, "Microsputterer with Integrated Ion-drag Focusing for Additive Manufacturing of Thin, Narrow Conductive Lines," *Journal of Physics D – Applied Physics*, vol. 51, no. 16, p. 165603, Apr. 2018.

Additively Manufactured Electro spray Ion Thrusters for Cubesats

D. Melo-Máximo, L. F. Velásquez-García

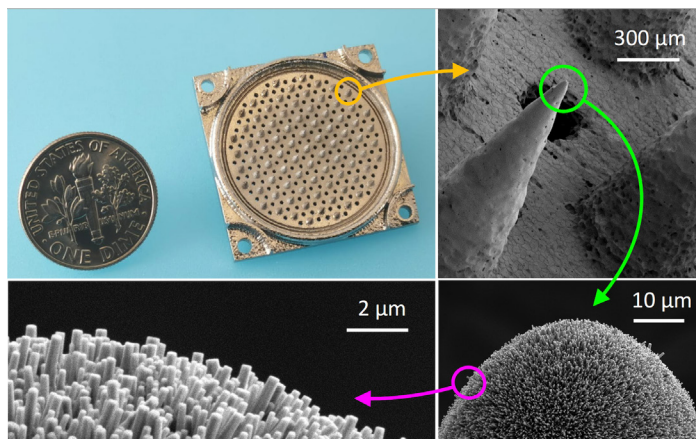
Sponsorship: MIT Portugal, MIT-Tecnologico de Monterrey Nanotechnology Program

Putting satellites in orbit is very expensive: typical rocket launches cost up to hundreds of millions of US dollars, and typical per-kilogram of payload costs are up to tens of thousands of US dollars). Therefore, great interest exists to develop smaller, lighter, and cheaper space satellites with adequate performance. In particular, since the 1990s, research groups across the world have been developing and launching cubesats, i.e., 1-10 Kg, a few L in volume, miniaturized, mission-focused satellites. Multi-material additive manufacturing is of great interest for fabricating cubesats, as it can monolithically create complex, multi-functional objects composed of freeform components made of materials matched to performance.

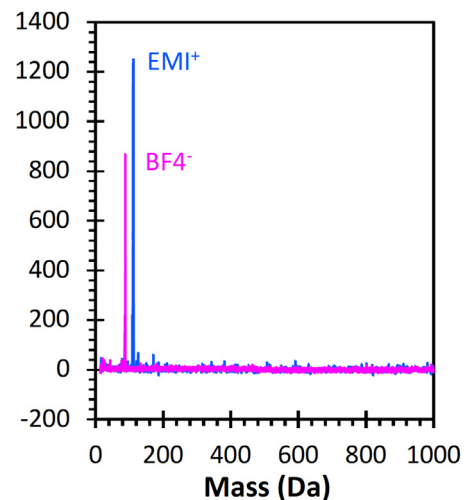
Electrospray engines produce thrust by electrohydrodynamically ejecting charged particles from liquid propellant. Electro spray thrusters are an attractive choice for propelling cubesats because their physics favors miniaturization, e.g., their start-up voltage scales with the square root of the emitter diameter. The thrust of an electro spray emitter is very

low; thus, electro spray engines have large arrays of emitters to greatly boost the thrust they can deliver.

We recently demonstrated the first additively manufactured electro spray engines. Our devices are composed of large arrays of conical emitters coated by a conformal forest of zinc oxide nanowires (ZnONWs) that transport the propellant to the emitter tips (Figure 1). The ZnONWs provide a large hydraulic impedance that regulates and uniformizes the flow across the emitter array, restricting the flow rate per emitter to attain ionic emission. Our devices are also remarkable because, unlike all the other electro spray ionic liquid engines reported in the literature, they emit only ions using the ionic liquid EMI-BF₄ as propellant (Figure 2), which maximizes their specific impulse for a given bias voltage, i.e., they produce more thrust per unit of propellant flow rate. Current work focuses on optimizing device design and fabrication and on developing a multi-electrode stack to control the plume.



▲ Figure 1: From the top left, clockwise: an additively manufactured electro spray array next to a U.S. dime, close-up of emitters, close-up of an emitter tip, close-up of the ZnONW forest.



▲ Figure 2: Mass spectra of emitted plume using EMI-BF₄ as propellant. In both polarities, the plume is composed exclusively of ions.

FURTHER READING

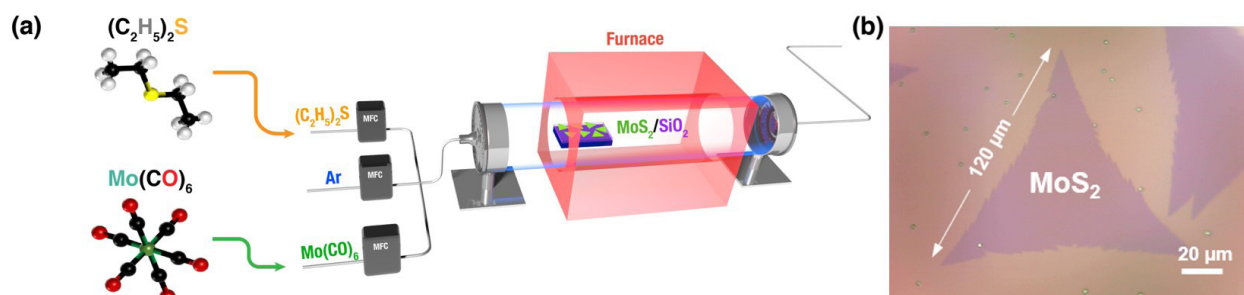
- F. A. Hill, E. V. Heubel, P. P. de Leon, and L. F. Velásquez-García, "High-Throughput Ionic Liquid Ion Sources Using Arrays of Microfabricated Electro spray Emitters with Integrated Extractor Grid and Carbon Nanotube Flow Control Structures," *J. Microelectromech. Syst.*, vol. 23, no. 5, pp. 1237-1248, May 2014.
- D. Olvera-Trejo and L. F. Velásquez-García, "Additively Manufactured MEMS Multiplexed Coaxial Electro spray Sources for High-Throughput, Uniform Generation of Core-Shell Microparticles," *Lab Chip*, vol. 16, no. 21, pp. 4121-4132, Oct. 2016.
- D. V. Melo Máximo and L. F. Velásquez-García, "Additively Manufactured Electrohydrodynamic Ionic Liquid Pure-Ion Sources for Nanosatellite Propulsion," *Additive Manufacturing*, vol. 36, p. 101719, Dec. 2020.

Low-Temperature Growth of High Quality MoS₂ by Metal-Organic Chemical Vapor Deposition

J.-H. Park, A.-Y. Lu, P.-C. Shen, J. Kong
Sponsorship: ARO MURI, NSF

The large-area and high-quality synthesis of molybdenum disulfide (MoS₂) plays an important role in realizing industrial applications of flexible, wearable, and ultimately scaled devices due to its atomically thin thickness, sizable bandgap, and dangling-bond-free interface. However, currently used synthesis of MoS₂ by chemical vapor deposition (CVD) require high temperature and a transfer process, which limits its utilization in device fabrications. In this work, we achieved the direct synthesis of high-quality monolayer MoS₂ by metal-organic chemical vapor deposition (MOCVD) at a low temperature of 320°C by designing the experimental setup for better controlling the flow rate of

the organic precursors. Large single-crystal monolayer MoS₂ with a domain size up to 120 μm can be obtained on SiO₂/Si substrate (Figure 1). Owing to the low substrate temperature, the MOCVD-grown MoS₂ exhibits low impurity doping and nearly unstrained properties on the growth substrate, demonstrating enhanced electronic performance with high electron mobility of 68.3 cm² V⁻¹s⁻¹ at room temperature. In addition, we propose a model to quantitatively analyze the shape change of the MoS₂ flakes grown under different conditions, which provides an insight into the growth mechanism for optimizing growth conditions.



▲ Figure 1: (a) Schematic diagram of the experimental setup of the MOCVD system for MoS₂ growth and (b) Optical image of MoS₂ flake grown on SiO₂/Si substrate at low temperature.

FURTHER READING

- J.-H. Park, A.-Y. Lu, P.-C. Shen, B. G. Shin, H. Wang, N. Mao, R. Xu, S. J. Jung, D. Ham, K. Kern, Y. Han, and J. Kong, "Synthesis of High-Performance Monolayer Molybdenum Disulfide at Low Temperature," *Small Methods*, submitted.
- K. Kang, S. Xie, L. Huang, Y. Han, P. Y. Huang, K. F. Mak, C.-J. Kim, D. Muller, and J. Park, "High-Mobility Three-Atom-Thick Semiconducting Films with Wafer-Scale Homogeneity," *Nature*, vol. 520, pp. 656-660, Apr. 2015.

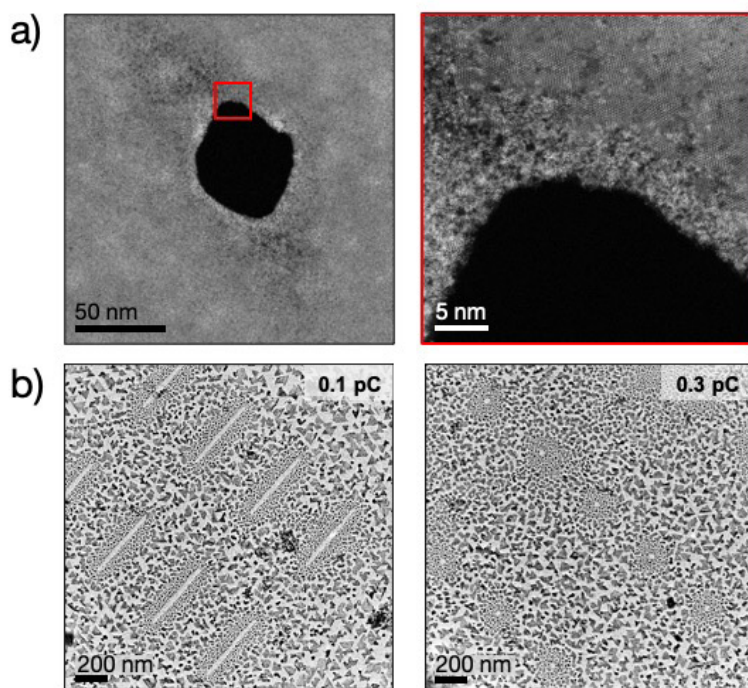
Self-Assembly via Defect-Mediated Metal Nanoisland Nucleation on 2D Materials

K. Reidy, V. Zarubin, Y. Yu, I. Charaev, J. D. Thomsen, F. M. Ross
Sponsors: MIT OGE, Mathworks Engineering, Microscopy Society of America (MSA)

Patterning point defects, nanopores, and nanoribbons can enhance (opto-)electronic properties of two-dimensional (2D) materials. Moreover, metal adatoms and small clusters can nucleate on point defects in 2D materials. This nucleation suggests that defect patterning may be used for templated self-assembly of metal nanoislands on 2D materials, enabling applications in plasmonics and single-photon emission. Focused ion beams (FIBs) are well-suited for patterning 2D materials with nanometer precision and can be used for the controlled creation of point defects and sub-10-nm features. For applications that require control of the locations of metal islands, the optimization of FIB irradiation parameters for metal nucleation is crucial.

In this work, we study the structural changes that arise from FIB patterning of suspended 2D materials and the influence of patterning on metal nucleation and growth. We calibrate the irradiation parameters

to achieve patterning with minimal damage to the 2D material, and the features are characterized by scanning transmission electron microscopy (STEM) (Figure 1a). Using these patterned 2D materials, we study the extent to which the defects, ion species, dose rate, and sample thickness affect the nucleation and growth of metals. Figure 1 shows representative results after the deposition of Au. At high deposition amounts, Au forms small islands around graphene nanopores, indicative of defect-mediated nucleation (Figure 1b). The templating and nucleation control presented here can be generalized to anchor other materials on 2D materials, such as Si and Ge via chemical vapor deposition or other metals via thermal and e-beam evaporation. This strategy opens routes towards the directed self-assembly of semiconducting and metallic nanoislands on 2D materials with optimized charge transfer and strong light-matter interactions.



◀ Figure 1: STEM characterization of defects and deposition on defective 2D materials. a) Defect in monolayer MoS₂ irradiated with He⁺ in the Helium Ion Microscope showing 50-nm hole created by ~600,000 He⁺ ions per spot irradiation. Right panel is a high magnification view of the amorphized region around a hole. b) Nucleation of Au islands on irradiated graphene flakes patterned with lines (left) and points (right), where Au appears as dark areas. Inset shows dose used.

FURTHER READING

- K. Reidy, G. Varnavides, J. D. Thomsen, A. Kumar, T. Pham, A.M. Blackburn, P. Anikeeva, P. Narang, J.M. LeBeau, F.M. Ross, "Direct Imaging and Electronic Structure Modulation of Moiré Superlattices at the 2D/3D Interface," *Nat. Comm.* vol. 12, pp. 1290, 2021, DOI:<https://doi.org/10.1038/s41467-021-21363-5>.
- J. Thomsen, K. Reidy, T. Pham, and F. M. Ross, "Nucleation and Growth of Metal Films and Nanocrystals on Two-dimensional Materials," *Microscopy and Microanalysis*, vol. 26, no. S2, pp. 1094-1096, 2020, DOI:10.1017/S1431927620016931.

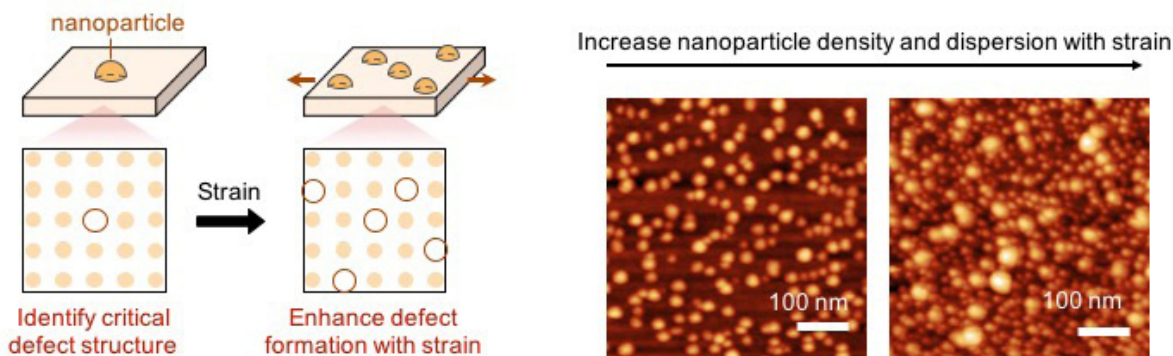
Strain Control of Nanocatalyst Synthesis

J. Wang, B. Yildiz
Sponsorship: Exelon Corporation

A central theme in renewable energy technologies today is designing nanostructured catalysts for desired reactions. Exsolution generates stable and catalytically active metal nanoparticles via phase precipitation out of a host oxide. Unlike traditional nanoparticle infiltration techniques, the nanoparticle catalysts from exsolution are anchored in the parent oxide. This strong metal-oxide interaction makes the exsolved nanoparticles more resistant against particle agglomeration than the infiltrated ones. While exsolution is an exciting and promising pathway for generating stable oxide supported nanoparticles, rational control over the exsolved particles has yet to be achieved. In particular, controlling the size and density of the exsolved nanoparticles remains a big challenge.

In this work, we propose point defect formation in the oxide lattice to be the fundamental knob to control exsolution and demonstrate this approach in epitaxial $\text{La}_{0.6}\text{Sr}_{0.4}\text{FeO}_3$ (LSF) thin films. By combining in-

situ surface characterization and ab-initio defect modeling, we show oxygen vacancy and Schottky defects to be the primary point defects formed upon FeO exsolution. Lattice strain tunes the formation energy, and thus the abundance of these defects, and alters the amount and size of the resulting exsolution particles. As a result, the tensile strained LSF with a facile formation of these critical point defects results in a higher FeO metal concentration, a larger density of nanoparticles, and reduced particle size at its surfaces. These observations highlight the critical role of point defects in controlling the size and density of the exsolved nanoparticles on the perovskite surface. The strain-controlled synthesis of nanocatalysts can benefit a wide range of applications in clean energy conversion and fuels generation such as solid oxide cells (SOCs), chemical looping (CL), and ceramic membrane reactors (CMRs).



▲ Figure 1: Schematics and atomic force microscopy images showing lattice strain can facilitate nanoparticle synthesis by tailoring point defect formation in the host oxide.

FURTHER READING

- J. Wang, B. Yildiz et al., "Tuning Point Defects by Strain Modulates Nanoparticle Exsolution on Perovskite Oxides," under review.

Controlled Cracking to Improve Mechanical Stability of RuO₂ Thin-Film Li-ion Electrodes

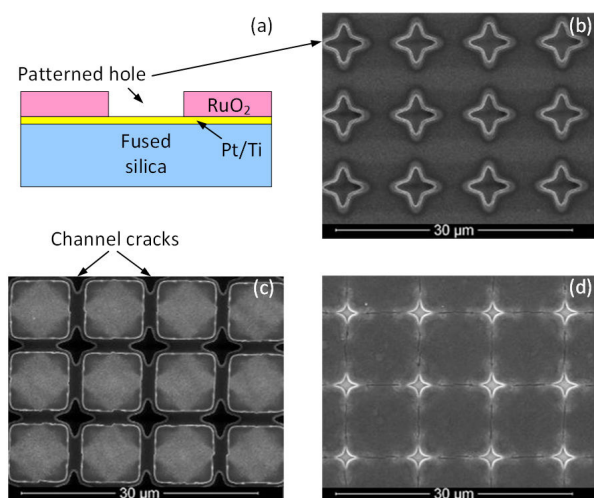
L. Xu, C. V. Thompson
Sponsorship: SMART

Thin film Li-ion batteries are of interest for low-cost autonomous sensors. We have investigated high-performance electrode materials, such as Si and Ge for anodes and RuO₂ for cathodes, that can reversibly store high concentrations of Li. RuO₂ is of particular interest as a cathode material because of its ability to reversibly store high concentrations of Li without requiring high-temperature processing, unlike conventional cathode materials. While high Li capacities are beneficial for high energy density, high Li concentrations lead to large volume changes, which can lead to mechanical degradation during battery cycling. In particular, removal of Li (delithiation) leads to tensile stresses that can cause cracking and delamination of electrodes, which can severely limit the number of times that batteries can be charged and discharged.

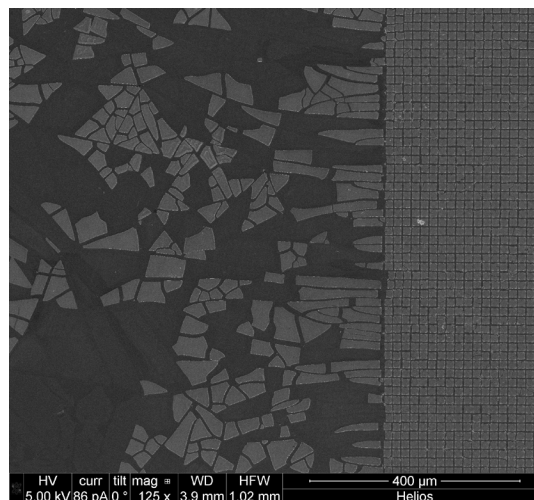
Motivated by the finding that patterned small patches of Si demonstrated higher mechanical stability compared to continuous films, patterned arrays of holes with stress-raising corners were fabricated within sputtered RuO₂ thin films (Figures 1a and b). After

lithiation and delithiation, channel cracks form along the directions defined by the hole array (Figure 1c). We found that this method for controlled crack formation led to increased mechanical stability, as no delamination occurred within the patterned area (Figure 2, right side), while severe delamination occurred in the unpatterned areas (Figure 2, left side). These results may occur because the formation of the controlled crack array dissipates the strain energy that would otherwise drive delamination.

It was further discovered that the formation of cracks was reversible. After re-lithiation, the RuO₂ patches expanded, and the channel cracks closed again (Figure 1d). The sizes of the channel cracks were controlled by the state of charge of the film. In addition to use for mechanical stabilization of thin film electrodes, this process has potential application for creation of channel networks with electrochemically modulated channel sizes, which might be of use in microfluidic devices.



▲ Figure 1: (a) Schematic cross-section and (b) top-view SEM image of a patterned RuO₂ film; (c) channel cracks formed after lithiation and delithiation and (d) channel cracks closed after re-lithiation.



▲ Figure 2: Comparison of unpatterned RuO₂ film (left side) and patterned film (right side) after cycling.

FURTHER READING

- D. Perego, J. S. T. Heng, X. Wang, Y. Shao-Horn, and C. V. Thompson, "High-performance Polycrystalline RuO_x Cathodes for Thin Film Li-ion Batteries," *Electrochim. Acta*, vol. 283, pp. 228–233, 2018.
- L. Xu and C. V. Thompson, "Mechanisms of the Cyclic (de)lithiation of RuO₂," *J. Mater. Chem. A*, vol. 8, pp. 21872–21881, 2020.

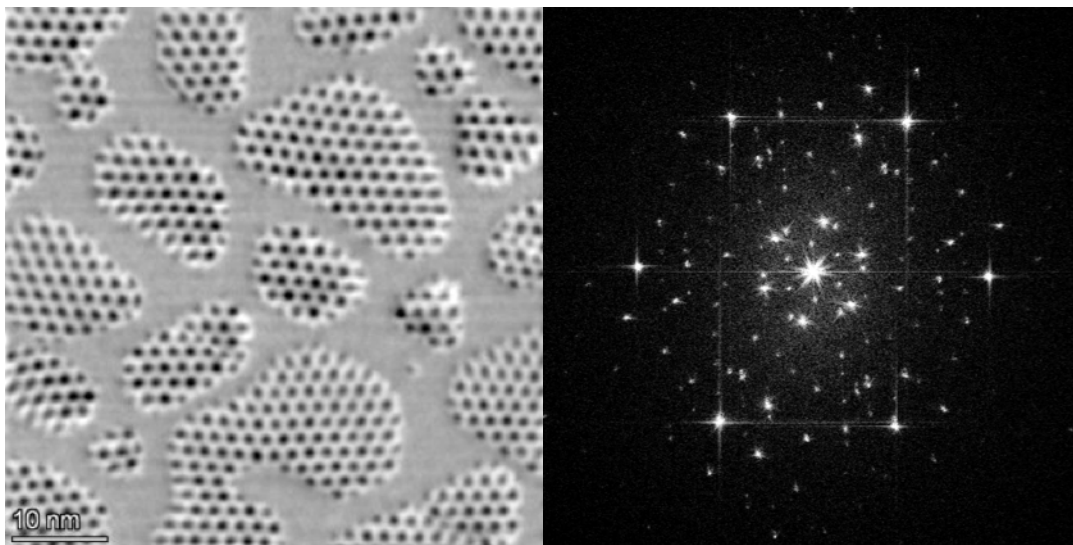
Seeing Superlattices: Imaging Moiré Periods at the Nanoisland-2D Material Interface Using Scanning Transmission Electron Microscopy

K. Reidy, G. Varnavides, J. Dahl Thomsen, A. Kumar, T. Pham, A. M. Blackburn, P. Anikeeva, P. Narang, J.M. LeBeau, F. M. Ross

Sponsorship: MIT MathWorks Engineering, MIT OGE, Office of Naval Research (ONR)

Opportunities are emerging to combine van der Waals (2D) materials with (3D) metals /semiconductors to explore fundamental charge-transport phenomena at their interfaces and exploit them for devices. Recent advances in scanning transmission electron microscopy (STEM) allow detailed analysis of atomic structure, properties, and ordering at these interfaces. We use 4D STEM and integrated differential phase contrast

(iDPC) to directly image moiré periodicities arising from epitaxial growth of nanoislands on 2D materials in ultra-high vacuum. Our research explores the role of emerging microscopy techniques in unveiling the alignment and ordering of moiré superlattices and the implications of moiré periodicities for the properties of 2D/3D junctions.



▲ Figure 1: Characterization of 2D/3D moiré superlattices: a) Integrated differential phase contrast (iDPC) STEM image of Au on MoS2 showcasing the moiré cells. b) Fast Fourier transform (FFT) of atomic resolution high-resolution TEM image of the Au on MoS2 showing $1/3\{422\}$ reflection and visible moiré periodicities around the central spot. Illustrative yellow dots represent frequencies from Au crystal planes, while purple represent frequencies from MoS2 crystal planes. Scale bar, 0.5 \AA^{-1}

FURTHER READING

- K. Reidy, et al., "Direct Imaging and Electronic Structure Modulation of Moiré Superlattices at the 2D/3D Interface," *Nat. Comm.* vol. 12, pp. 1290, 2021, DOI:<https://doi.org/10.1038/s41467-021-21363-5>

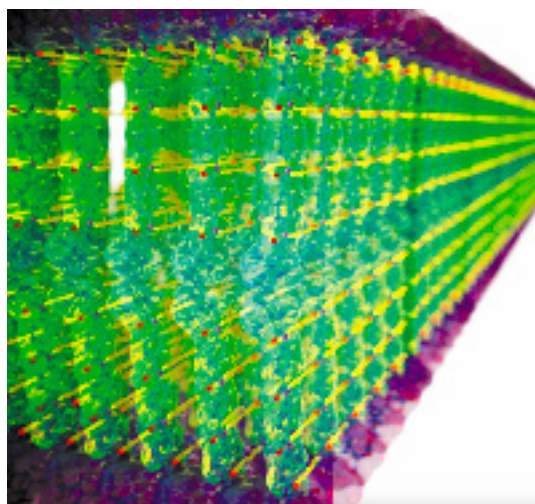
Small-Molecule Assemblies Inspired by Kevlar: Aramid Amphiphile Nanoribbons

T. Christoff-Tempesta, Y. Cho, D.-Y. Kim, J.H. Ortony

Sponsorship: NSF, J-WAFS, Professor Amar G. Bose Research Grant Program

Small-molecule self-assembly offers a powerful bottom-up approach to producing nanostructures with high surface areas, tunable surfaces, and defined internal order. Historically, the dynamic nature of these systems has limited their use to specific cases, especially biomedical applications, in solvated environments. Here, we present a self-assembling small-molecule platform, the aramid amphiphile (AA), which overcomes these dynamic limitations. AAs incorporate a Kevlar-inspired domain within each molecule to produce strong interactions between molecules. We ob-

serve that AAs spontaneously form nanoribbons when added to water with aspect-ratios exceeding 4000:1. Robust internal interactions suppress the ability of AAs to move between assemblies and result in nanoribbons with mechanical properties rivaling silk. We harness this stability to extend small-molecule assemblies to the solid-state for the first time, forming macroscopic threads that are easily handled and support 200 times their weight when dried. The AA platform offers a novel route to use small-molecule self-assembly to achieve aligned nanoscale materials in the solid-state



▲ Figure 1: Illustration of a nanoribbon constructed from the spontaneous self-assembly of aramid amphiphiles in water, with strong hydrogen bonding interactions between molecules shown in yellow.

FURTHER READING

- T. Christoff-Tempesta, Y. Cho, D.-Y. Kim, M. Geri, G. Lamour, A.J. Lew, X. Zuo, W.R. Lindemann, and J.H. Ortony, "Self-assembly of Aramid Amphiphiles into Ultra-stable Nanoribbons and Aligned Nanoribbon Threads," *Nature Nanotechnology*, vol. 16, pp. 447-454, January 2021
- T. Christoff-Tempesta, D.-Y. Kim, G. Lamour, X. Zuo, K.-H. Ryu, and J.H. Ortony, "Morphological Transitions of a Photoswitchable Aramid Amphiphile Nanostructure," *Nano Letters*, vol. 21, pp. 2912-2918, March 2021
- T. Christoff-Tempesta and J.H. Ortony, "Aramid Amphiphile Nanoribbons for the Remediation of Lead from Contaminated Water," *Environmental Science: Nano*, May 2021